Out-of-the-groove transport of lipids by TMEM16 and GPCR scramblases

Mattia Malvezzi[a], Kiran K. Andra[b], Kalpana Pandey[b], Byoung-Cheol Lee[a], Maria E. Falzone[b], Ashley Brown[b], Rabia Iqbal[b], Anant K. Menon[b], and Alessio Accardi[a,b,c,1]

[a]Department of Anesthesiology, Weill Cornell Medical College, New York, NY 10065; [b]Department of Biochemistry, Weill Cornell Medical College, New York, NY 10065; and [c]Department of Physiology and Biophysics, Weill Cornell Medical College, New York, NY 10065

Edited by Christopher Miller, Howard Hughes Medical Institute and Brandeis University, Waltham, MA, and approved May 25, 2018 (received for review April 18, 2018)

Phospholipid scramblases externalize phosphatidylserine to facilitate numerous physiological processes. Several members of the structurally unrelated TMEM16 and G protein-coupled receptor (GPCR) protein families mediate phospholipid scrambling. The structure of a TMEM16 scramblase shows a membrane-exposed hydrophilic cavity, suggesting that scrambling occurs via the "credit-card" mechanism where lipid headgroups permeate through the cavity while their tails remain associated with the membrane core. Here we show that afTMEM16 and opsin, representatives of the TMEM16 and GCPR scramblase families, transport phospholipids with polyethylene glycol headgroups whose globular dimensions are much larger than the width of the cavity. This suggests that transport of these large headgroups occurs outside rather than within the cavity. These large lipids are scrambled at rates comparable to those of normal phospholipids and their presence in the reconstituted vesicles promotes scrambling of normal phospholipids. This suggests that both large and small phospholipids can move outside the cavity. We propose that the conformational rearrangements underlying TMEM16- and GPCR-mediated credit-card scrambling locally deform the membrane to allow transbilayer lipid translocation outside the cavity and that both mechanisms underlie transport of normal phospholipids.

membrane | scrambling | phospholipids | channel | opsin

Ca^{2+}-dependent phospholipid scramblases collapse the lipid asymmetry of the plasma membrane by moving phospholipids bidirectionally down their chemical gradients. This exposes phosphatidylserine (PS) at the cell surface, which is crucial for processes such as blood coagulation, phagocytosis of apoptotic cells, and bone formation (1–4). Members of three unrelated families of membrane proteins, rhodopsin-like class-A G protein-coupled receptors (GPCR) and Xk-related (Xkr) and TMEM16 proteins, have been shown to scramble phospholipids (5–13). GPCRs such as opsin and β-adrenergic receptors were shown to be Ca^{2+}-independent phospholipid scramblases (5, 6), while Xkr4, 8, and 9 were reported to function as caspase-activated scramblases mediating proapoptotic externalization of PS (7, 8, 12, 14). However, despite recent progress (15, 16) the mechanism by which the GPCRs and Xk-related proteins mediate lipid scrambling is not well understood. In contrast, structural, functional, and computational studies of the TMEM16 family have identified key regions that control transport and Ca^{2+} regulation (10, 11, 17–19). The TMEM16 family comprises dual-function Ca^{2+}-dependent channels/scramblases and Ca^{2+}-activated Cl^- channels (10, 11, 20–25). To date four family members, the human TMEM16E and TMEM16F proteins and the fungal afTMEM16 and nhTMEM16 proteins, have been shown to be channels/scramblases (4, 10, 25–28). The crystal structure of nhTMEM16 revealed that these proteins are dimers (Fig. 1*A*) where each monomer forms a ∼10-Å membrane-exposed hydrophilic groove-like cavity (Fig. 1*B*) that could provide a translocation pathway for lipids (11). The suggested scrambling mechanism (11, 17) resembles the previously proposed "credit-card" mechanism (29, 30) where the lipid headgroups enter and interact with the cavity while their hydrophobic acyl chains remain in the core of the membrane (Fig. 1*C*). This mechanism elegantly explains how the energy barrier for lipid headgroup translocation across the hydrophobic membrane core is lowered by TMEM16 scramblases, and how the observed fast rates of phospholipid scrambling can be achieved. This model would also apply to lipid-scrambling GPCRs that can dynamically form a hydrophilic cavity-like structure (16). However, the presence of a long, proteinaceous membrane-traversing channel through which headgroups permeate is difficult to reconcile with the poor selectivity of scramblases (10, 11, 31). These observations raise two key questions. First, do TMEM16 proteins translocate lipids strictly via the hydrophilic cavity? For example, it has been proposed that these proteins deform and thin the membrane in the vicinity of the groove (18, 32, 33), potentially allowing lipid movement outside the cavity. Second, can such an out-of-the-cavity scrambling mechanism also apply to other scramblases? The observation that the GPCR opsin is able to scramble a glycosylphosphatidylinositol lipid with a large headgroup (>1,000 Da) lends credence to this possibility (6).

If lipid transport by TMEM16 scramblases can only occur via permeation of the headgroup through the groove, then lipids with headgroups larger than the groove should be excluded. In

Significance

The plasma membrane of all eukaryotic cells is asymmetric, with the signaling lipid phosphatidylserine in the cytoplasmic leaflet. When activated, membrane proteins termed phospholipid scramblases collapse this asymmetry by exchanging lipids between bilayer leaflets. The resulting externalization of phosphatidylserine is needed for phagocytosis of apoptotic cells, blood coagulation, and membrane repair. The mechanism by which scramblases transport lipids is poorly understood. The structure of a TMEM16-scramblase suggested that phospholipid headgroups move through a membrane-exposed hydrophilic groove, as a credit card moves through a card reader. Here we show that TMEM16 and GPCR scramblases transport lipids with very large headgroups, suggesting an out-of-the-groove transport mechanism. We propose that scramblases locally deform the membrane to translocate lipids both within and outside the groove.

Author contributions: M.M., A.K.M., and A.A. designed research; A.K.M. introduced the concept to use PEGylated lipids to size the lipid pathway; K.K.A., A.B., R.I., and A.K.M. designed and synthesized the PEGylated lipids; M.M. and B.-C.L. performed TMEM16 scrambling experiments; K.P. performed the opsin scrambling experiments; M.E.F. performed EM data acquisition; A.A. designed and implemented data analysis; M.M. and A.A. analyzed data; and M.M., A.K.M., and A.A. wrote the paper.

The authors declare no conflict of interest.

This article is a PNAS Direct Submission.

[1]To whom correspondence should be addressed. Email: ala2022@med.cornell.edu.

This article contains supporting information online at www.pnas.org/lookup/suppl/doi:10.1073/pnas.1806721115/-/DCSupplemental.

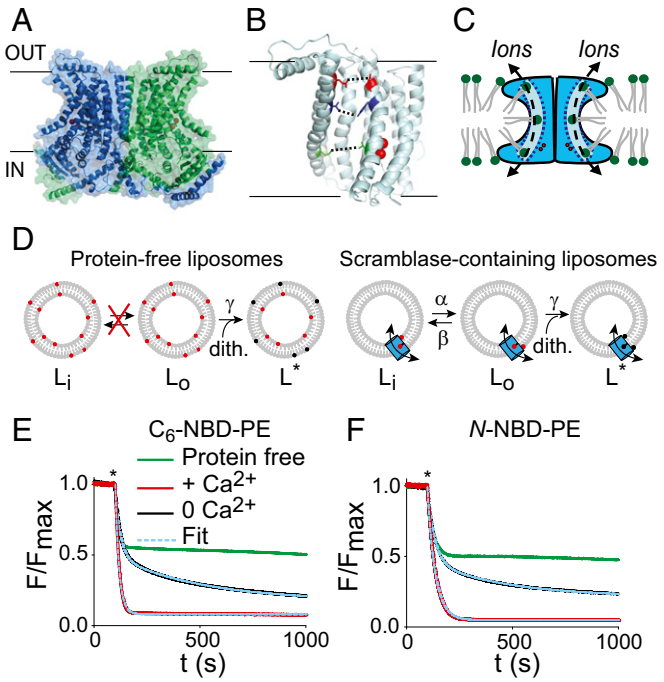

Fig. 1. Phospholipid scrambling of NBD-PE lipids by afTMEM16. (*A*) Ribbon and surface representations of the nhTMEM16 dimer (11), viewed from the plane of the membrane. Single monomers are colored green and blue, and bound Ca^{2+} ions are shown as red spheres. The lines represent the membrane boundary. (*B*) The hydrophilic cavity viewed from the plane of the membrane (11). The width of the cavity is measured at three positions using the side chains of three pairs of residues in TM4 and TM6: Q326 - N435 (red), 12.34 Å; T333 – Y439 (blue), 7.03 Å; M348 – T451 (green), 16.40 Å. Helices not involved in the cavity were removed for clarity. (*C*) Schematic model for credit-card scrambling mechanism by nhTMEM16. (*D*) Schematic representation of the dithionite-based scrambling assay. NBD-lipids (red) are irreversibly reduced (black) by dithionite. In PF liposomes (*Top*) only outer-leaflet fluorophores are reduced while in afTMEM16-containing proteoliposomes (*Bottom*) NBD lipids are translocated to the outer leaflet and thus all fluorophores are reduced (only one NBD-lipid is shown for clarity). (*E* and *F*) Representative traces of the time course of the fluorescence reduction in afTMEM16-containing liposomes reconstituted with 0.5 mol % C_6-NBD-PE (*E*) or *N*-NBD-PE (*F*) with 0.5 mM Ca^{2+} (red) or 0 mM Ca^{2+} (black). Green traces represent PF liposomes. Dashed cyan lines represent fits to Eq. **5** (with 0.5 mM Ca^{2+}, red traces) or Eq. **4** (0 mM Ca^{2+}, black traces). Asterisk denotes the addition of sodium dithionite.

contrast, if scrambling can also occur outside the cavity then lipids with bulkier headgroups might be transported. Therefore, we tested whether and how lipids conjugated to large globular PEG molecules, approximately four times the width of the cavity, are scrambled by afTMEM16. We found that PEGylated lipids are scrambled by afTMEM16 in a Ca^{2+}-dependent manner at rates that are only approximately twofold slower than those of regular phospholipids. Raising the concentration of these PEGylated lipids increased the rate at which they were scrambled while also increasing the scrambling rate of normal phospholipids, suggesting that all phospholipids can be scrambled outside of the groove. In contrast, the presence of these lipids did not affect ion permeation through afTMEM16, suggesting that ion movement is constrained by the groove. We then asked whether other types of scramblases can also scramble PEGylated lipids. We found that the GPCR opsin also efficiently scrambles the PEG-conjugated lipids despite the absence of a crystallographically evident transbilayer groove, at rates that exceed those of afTMEM16. Taken together our results show that the membrane-exposed cavity of the TMEM16 scramblases does not impose a cutoff on headgroup size. Our data suggest that the conformational changes underlying opening of the lipid-translocation groove of the TMEM16- and GPCR-type scramblases induce local membrane rearrangements that provide an additional mechanism for transbilayer lipid movement. Thus, credit-card scrambling is supplemented by an out-of-the-groove mechanism for TMEM16 and GPCR scramblases.

Results

Our goal was to investigate whether the lipid-facing groove in TMEM16 proteins imposes a size cutoff such that phospholipids with headgroups larger than a particular size would not be translocated. To do this we generated a nested set of phosphatidylethanolamine (PE) lipids labeled with nitrobenzoxadiazole (NBD) and with PEG headgroups of increasing size (*SI Appendix*, Fig. S1*A*) and measured whether and how afTMEM16 transports these lipids. We tested lipids with headgroups that are much larger than the widest point of the cavity (Fig. 1*B*).

Generation, Characterization, and Reconstitution Properties of NBD-Labeled PEGylated Lipids. All tested lipids had NBD-labeled headgroups, except for C_6-NBD-PE in which the NBD fluorophore was attached to a short 2-acyl chain (*SI Appendix*, Fig. S1*A*, C_6-NBD-PE). The NBD fluorophore was conjugated to the free amine of the PE headgroup (*SI Appendix*, Fig. S1*A*, *N*-NBD-PE), or to that of amino-PEG of average molecular mass 2, 3.4, or 5 kDa conjugated to the PE headgroup (*SI Appendix*, Fig. S1*A*, PE-PEGX-NBD, where X = molecular mass). The PE-PEGX-NBD lipids were characterized by TLC (*SI Appendix*, Fig. S2*A*) and MALDI-TOF mass spectrometry (*SI Appendix*, Fig. S2*B*). Dynamic light scattering (DLS) measurements of the PEGX headgroups released by deacylation of the phospholipids (34) show that all three molecules have a size frequency distribution pattern characterized by a single major peak, with average diameters of 2.5, 3.5, and 4.2 nm for PEG2000, PEG3400, and PEG5000, respectively (*SI Appendix*, Fig. S1*B*).

We reconstituted the five NBD-labeled lipids into large unilamellar vesicles at a ratio of 0.5 mol % of total lipids and measured the rate of NBD reduction by 20 mM extraliposomal sodium dithionite. Dithionite is a reducing agent that irreversibly converts the nitro group of the NBD fluorophore to an amino group, rendering the molecule nonfluorescent. For protein-free (PF) vesicles the decay of fluorescence reflects bleaching of the outer-leaflet NBD-labeled lipids and can be described by the following Markov model (Fig. 1*D*, *Left*):

$$L_i^{PF} \quad L_o \xrightarrow{\gamma} L^*, \qquad \text{(Scheme 1)}$$

where $L^{PF}{}_i$ are the fluorescent NBD-labeled lipids in the inner leaflet of a membrane which are protected by dithionite. The NBD-labeled lipids in the outer leaflet, L_o, are accessible to dithionite and therefore can be reduced to their nonfluorescent form L^*; γ is the pseudo-first-order rate constant of dithionite reduction of an NBD fluorophore conjugated to a lipid so that $\gamma = [D]\gamma'$, where [D] is the dithionite concentration and γ′ is the second-order rate constant for dithionite reduction. In all cases the fluorescence decay could be well described by a single exponential function (Eq. **2** and *SI Appendix*, Fig. S1*C*). As previously reported, C_6-NBD-PE and *N*-NBD-PE are reduced more slowly than soluble NBD-Glucose (*SI Appendix*, Fig. S1*C* and Table S1), with pseudo-first-order reduction rate constants of ∼0.065 s^{-1} and 0.035 s^{-1}, respectively, compared with 1.9 s^{-1} for NBD-Glucose, indicating that the close proximity of the fluorophore to the membrane surface slows the bleaching reaction (6, 10). The plateau fluorescence level was ∼50% (*SI Appendix*, Fig. S1*E* and Table S1), consistent with the expectation that the lipids distribute symmetrically between the two leaflets. Dithionite entry into the liposomes is negligible under our experimental conditions

and time scale (10). Interestingly, PE-PEG2000/3400/5000-NBD lipids show faster reduction kinetics, with rate constants of ~1 s^{-1} (*SI Appendix*, Fig. S1 *C* and *D* and Table S1), close to that measured for NBD-Glucose. The NBD fluorophores in these lipids may be more accessible to dithionite because they are further away from the membrane. Also, while PE-PEG2000-NBD distributes nearly equally between the leaflets (*SI Appendix*, Fig. S1*E* and Table S1), PE-PEG3400/5000-NBD distribute slightly asymmetrically with a preference for the outer leaflet (*SI Appendix*, Fig. S1*E* and Table S1).

We investigated whether incorporation of the PEGylated lipids alters the size or stability of the liposomes. We prepared PF liposome samples by extrusion through a 400-nm membrane before analysis, as we do for proteoliposomes, and found that that they have a mean diameter of ~200 nm (*SI Appendix*, Fig. S1*F*). Addition of 0.5% PE-PEG2000, PE-PEG3400, or PE-PEG5000 induced minor changes in the distributions with means of 195, 180, and 185 nm, respectively (*SI Appendix*, Figs. S1*F* and S3*C*). The mean diameter of liposomes containing 5% PE-PEG2000 was ~260 nm but still within the variance of the distributions (*SI Appendix*, Figs. S1*F* and S3*C*). Similarly, the total amount of Cl^- trapped in PF liposomes, a measure of liposome volume, was not significantly affected by the addition of 0.5–5% PEGylated lipids (*SI Appendix*, Fig. S1*G*), suggesting that the liposomal membranes maintain their integrity. To further probe whether addition of 0.5–5% PEGylated lipids affects liposome stability and integrity, we used cryoelectron microscopy to visualize the vesicles directly (*SI Appendix*, Fig. S3 *A* and *B*). In all conditions, the liposomes are nearly round and their membranes continuous, indicating that addition of the PEGylated lipids at concentration <5% does not affect their integrity. Further, the vesicles reconstituted in the 5% conditions have similar distributions (*SI Appendix*, Fig. S3 *B* and *C*). In cryoimaging conditions the grid holes are covered by thin ice, ~150–200 nm, placing a physical constraint on the size of the captured liposomes (35). As expected, this skews the size distribution toward smaller vesicles compared with that seen in the DLS experiments (*SI Appendix*, Fig. S3 *B* and *C*). Notably, the presence of smaller vesicles inside the larger vesicles partially rationalizes our previous finding that there is a population of liposomes that is protected from dithionite (10). Taken together, these analyses show that addition of 0.5–5% PEGylated lipids to the liposomes does not affect their size or integrity.

A Quantitative Description of Lipid Scrambling by TMEM16 Scramblases. Scrambling by two fungal TMEM16 homologs, afTMEM16 (10, 25) and nhTMEM16 (11), has been investigated using the dithionite reduction assay (6). However, a method to quantify the rates of scrambling by these proteins was lacking. Here, we developed an analytical description of the time course of fluorescence decay induced by the addition of dithionite, which in scramblase-containing vesicles is described by a three-state Markov model (Scheme 2) (Fig. 1*D*, *Right*) (36):

$$L_i \underset{\beta}{\overset{\alpha}{\rightleftarrows}} L_o \xrightarrow{\gamma} L^*. \qquad \text{(Scheme 2)}$$

In agreement with past results, in the presence of Ca^{2+} the fluorescence decay of C_6-NBD-PE and *N*-NBD-PE in afTMEM16 vesicles occurs with kinetics comparable to those of PF liposomes (Fig. 1 *E* and *F*), indicating that our detection of scrambling is rate-limited by the chemical reduction of the NBD fluorophores. Indeed, when fitting the fluorescence decay to Eq. **5**, α cannot be uniquely determined and only a lower limit of $\alpha(+Ca^{2+}) \sim \beta(+Ca^{2+}) > 0.2\ s^{-1}$ can be determined for both lipids (*SI Appendix*, Fig. S4 and Table S1). In contrast, in the absence of Ca^{2+}, bleaching of both lipids occurs with biexponential kinetics, with the fast component reflecting the chemical step and the slow one corresponding to lipid scrambling (Fig. 1 *E* and *F*) (10). Correspondingly, the traces in 0 Ca^{2+} can be well fit by Eq. **5** and yield comparable scrambling rate constants of $\alpha(0\ Ca^{2+}) \sim \beta(0\ Ca^{2+}) \sim 0.001$–$0.003\ s^{-1}$ (Figs. 1 *E* and *F* and 2 *E* and *F* and *SI Appendix*, Table S1). Comparable results were obtained for nhTMEM16 which scrambles *N*-NBD-PE with Ca^{2+}-dependent rate constants of $\alpha^{nh}(+Ca^{2+}) \sim \beta^{nh}(+Ca^{2+}) > 0.2\ s^{-1}$ and $\alpha^{nh}(0\ Ca^{2+}) \sim \beta^{nh}(0\ Ca^{2+}) \sim 0.001\ s^{-1}$ (Fig. 2 *E* and *F* and *SI Appendix*, Fig. S5*A* and Table S2) Therefore, binding of Ca^{2+} to afTMEM16 and nhTMEM16 increases the scrambling rate of C_6-NBD-PE and *N*-NBD-PE by >200-fold.

afTMEM16 Scrambles PEGylated Lipids. We next tested whether PE derivatives with large headgroups, PE-PEG2000/3400/5000-NBD, are scrambled by afTMEM16. We found that these lipids are scrambled nearly as well as the much smaller C_6-NBD-PE and *N*-NBD-PE (Fig. 2 *A*–*C*): in the presence of Ca^{2+}, scrambling of all PEG-conjugated lipids plateaus at values comparable to NBD-PE lipids (Fig. 2*D*) and with rapid kinetics (Fig. 2*E*). In the absence of Ca^{2+} (Fig. 2 *A*–*C*) the scrambling kinetics are slower (Fig. 2*F*), indicating that these large PEGylated lipids are transported by afTMEM16 in a Ca^{2+}-dependent manner. The time course of fluorescence decay of the PE-PEGX-NBD lipids is biexponential both in the presence and absence of Ca^{2+} (Fig. 2 *A*–*C*), with the fast component close to the rate of dithionite bleaching measured in PF liposomes containing these lipids (*SI Appendix*, Fig. S1*C*). Indeed, reducing the amount of dithionite from 20 mM to 2.5 mM slows down this process by approximately threefold in PF and proteoliposomes in the presence of Ca^{2+}, $\gamma(20\ mM) \sim 0.9\ s^{-1}$ to $\gamma(2.5\ mM) \sim 0.3\ s^{-1}$ (*SI Appendix*, Fig. S6), allowing us to assign this component unambiguously to the chemical step. The presence of a component slower than the chemical step even in the presence of Ca^{2+} indicates that we can directly measure lipid scrambling in the presence of ligand. The fluorescence decay of PE-PEG2000-NBD in saturating Ca^{2+} can be well fit to Eq. **5** (Fig. 2*A*), with $\alpha \sim \beta \sim 0.1\ s^{-1}$ (Fig. 2*E* and *SI Appendix*, Table S1), indicating that afTMEM16 scrambles this large lipid at a rate that is approximately twofold slower than the rate of the normal PE lipids (Figs. 1 *E* and *F* and 2*E*). Removal of Ca^{2+} slows down scrambling by ~100-fold to $\alpha \sim \beta \sim 0.001\ s^{-1}$, a value comparable to that of normal PE lipids (Fig. 2*F* and *SI Appendix*, Table S1). This supports the notion that scrambling of the PEGylated lipids is a general property of TMEM16 scramblases. A similar analysis carried out for the scrambling of PE conjugated to the even larger PEG3400 and PEG5000 shows that both are scrambled by afTMEM16 at rates that are increased >100 times Ca^{2+} binding and are comparable to those of the regular-sized PE lipids (Fig. 2 *E* and *F*). It is worth noting that for PE-PEG3400-NBD and PE-PEG5000-NBD the scrambling rate in the presence of Ca^{2+} is rate-limited by the chemical reduction step, indicating that afTMEM16 scrambles these large molecules faster than PE-PEG2000-NBD (*SI Appendix*, Table S1). In the remainder of this work we use PE-PEG2000-NBD, as for this lipid we can resolve the scrambling rates both in the presence and absence of Ca^{2+}.

Recent work has brought into light the conformational changes that regulate opening of the TMEM16 groove. The cryoelectron microscopy structures of the TMEM16A channel homolog revealed that Ca^{2+} gating involves the movement of the intracellular portion of the pore-lining TM6 helix (37, 38). We and others identified a network of polar residues located at the extracellular entryway of the nhTMEM16 groove that is important for lipid recruitment (18, 33, 39) and that undergoes a conformational rearrangement to allow the groove to open, enabling penetration of the lipid headgroups and scrambling (39). We reasoned that if all lipids permeate through the groove, then impairing either conformational change should affect their scrambling rates to the same extent. Thus, to probe whether and how the conformational rearrangements of the groove regulate

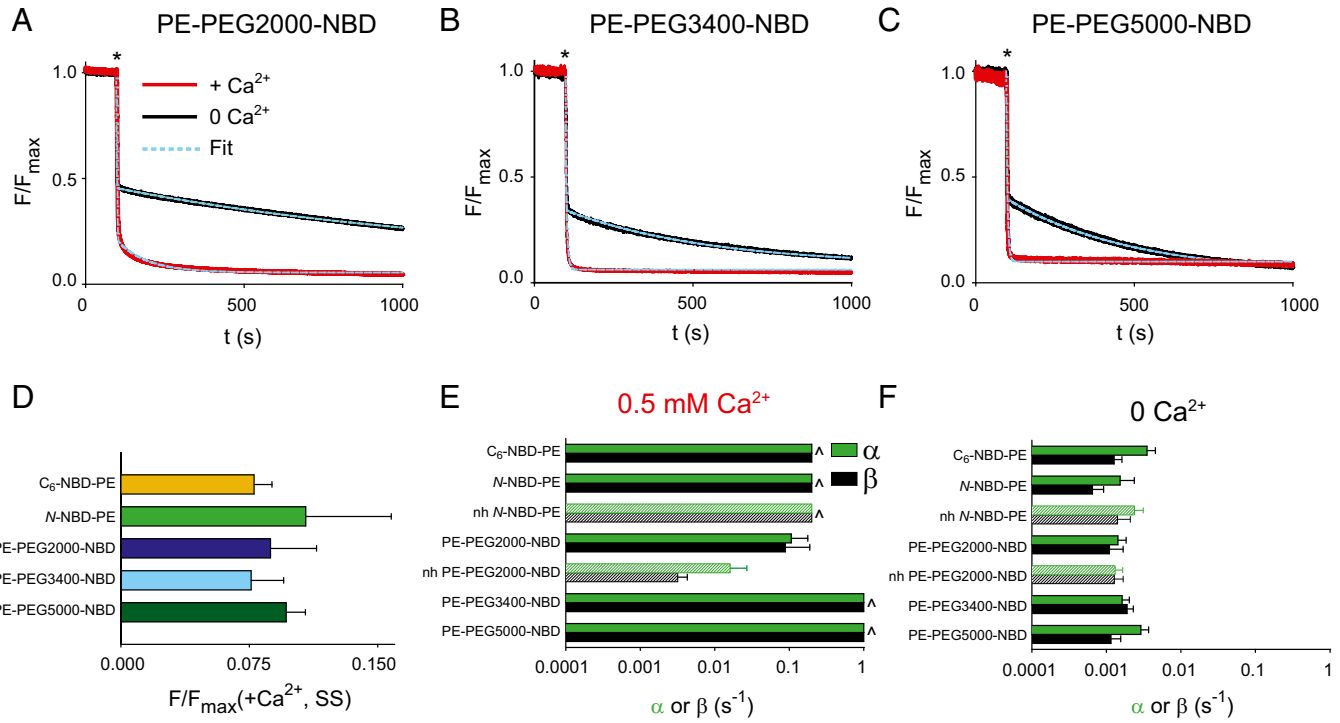

Fig. 2. Phospholipid scrambling of PEG-conjugated lipids by afTMEM16. (*A–C*) Representative traces of the time course of the fluorescence reduction in afTMEM16-containing liposomes reconstituted with 0.5 mol % PE-PEG2000-NBD (*A*), PE-PEG3400-NBD (*B*), or PE-PEG5000-NBD (*C*) with 0.5 mM Ca^{2+} (red) or 0 mM Ca^{2+} (black). Dashed cyan lines represent fits to Eqs. **4** or **5**. Asterisk denotes the addition of sodium dithionite. (*D*) Average normalized steady-state fluorescence of afTMEM16-containing liposomes reconstituted with 0.5 mol % C_6-NBD-PE (orange, $n = 16$), *N*-NBD-PE (red, $n = 13$), PE-PEG2000-NBD (blue, $n = 18$), PE-PEG3400-NBD (cyan, $n = 9$), or PE-PEG5000-NBD (dark green, $n = 10$) in the presence of 0.5 mM Ca^{2+}. (*E* and *F*) Scrambling rate constants, α (green) and β (black), obtained by fitting the fluorescence time courses with 0.5 mM Ca^{2+} (*E*) or 0 mM Ca^{2+} (*F*) to Eq. **4** for afTMEM16 (solid bars) and nhTMEM16 (dashed bars). ^ denotes where α = β was imposed and constrained as described in *SI Appendix*, Fig. S4, and Eq. **5** was used (*SI Appendix*, *Appendix 1* and Table S1). Data are mean ± SD.

scrambling of the PEG-conjugated lipids we investigated whether Ca^{2+}-dependent gating or opening of the extracellular gate of the groove are required for their transport.

We first tested how the Ca^{2+}-insensitive double mutant D511A/E514A of afTMEM16 (10) affects scrambling of normal and PEGylated lipids. The D511A/E514A mutant scrambles *N*-NBD-PE in a Ca^{2+}-independent manner at a rate similar to that of the WT protein in the absence of Ca^{2+}, α(DA/EA) ~ 0.001 s^{-1} (Fig. 3 *A* and *C* and *SI Appendix*, Table S1). Thus, in afTMEM16 the same Ca^{2+}-dependent conformational change regulates scrambling of regular and PEG-conjugated phospholipids.

We next confirmed that nhTMEM16 was able to scramble PE-PEG2000-NBD lipids similarly to afTMEM16 (Fig. 3 *E* and *F* and *SI Appendix*, Fig. S5*B*). When we tested whether the external-gate-impairing mutant R432W of nhTMEM16 scrambles PEGylated lipids (39), we found scrambling of the smaller *N*-NBD-PE is preferentially impaired compared with the large PE-PEG2000-NBD (Fig. 3 *D–F*). Thus, the R432W mutant reduces the forward and backward scrambling rate constants of *N*-NBD-PE by >100-fold, from >0.2 s^{-1} to ~2×10^{-3} s^{-1} (Fig. 3*F* and *SI Appendix*, Table S2). In contrast, the mutant reduces the forward scrambling rate constant of the large PE-PEG2000-NBD lipid by only 8.9-fold (from 16×10^{-3} s^{-1} to 1.8×10^{-3} s^{-1}), and the reverse rate constant by ~1.5-fold (from 3.2×10^{-3} s^{-1} to 2.3×10^{-3} s^{-1}) (Fig. 3*F* and *SI Appendix*, Table S2). Therefore, the R432W mutation affects scrambling of the small *N*-NBD-PE lipid 10–100 times more than that of the larger PE-PEG2000-NBD. Importantly, in the absence of Ca^{2+} the R432W mutant impairs scrambling of *N*-NBD-PE and PE-PEG2000-NBD to the same extent (Fig. 3*F* and *SI Appendix*, Table S2), consistent with the idea that the conformational rearrangement regulated by R432 occurs downstream of Ca^{2+} binding (39). These results support the hypothesis that scrambling of the PEG-conjugated lipids does not require their penetration deep within the cavity.

Scrambling of PEGylated lipids occurs at rates somewhat slower or comparable to those of a "normal" PE lipid, and the same Ca^{2+}-dependent conformational change regulates transport of all lipids. These results are difficult to reconcile with the credit-card model (Fig. 1*C*) in which scrambling occurs only when the lipid headgroup fits within the groove. Rather, our findings raise the possibility that scrambling of the PEGylated lipids might also occur outside the groove. Consistent with this possibility is our observation that transport of PE-PEG2000-NBD is less impaired than that of *N*-NBD-PE in the R432W mutant that prevents opening of the extracellular gate of the groove (39). We envisage that out-of-the-groove lipid transport is enabled by groove-dependent local distortions and thinning of the membrane in the vicinity of the protein. This hypothesis is consistent with the finding that the nhTMEM16 scramblase induces a pronounced membrane thinning in the proximity of the groove in molecular dynamics calculations (18, 33). An alternative interpretation of these results is that the groove could dilate to accommodate these very large headgroups, which would require a major rearrangement induced by the permeating PEGylated lipids.

Scrambling of PEG-Conjugated Lipids Does Not Alter Ion Conduction by afTMEM16. To investigate whether scrambling of large lipids alters the physical dimensions of the cavity we investigated how the ion conduction properties of afTMEM16 are affected by the presence of permeating PEGylated lipids. We previously showed that afTMEM16, like other TMEM16-family scramblases, also

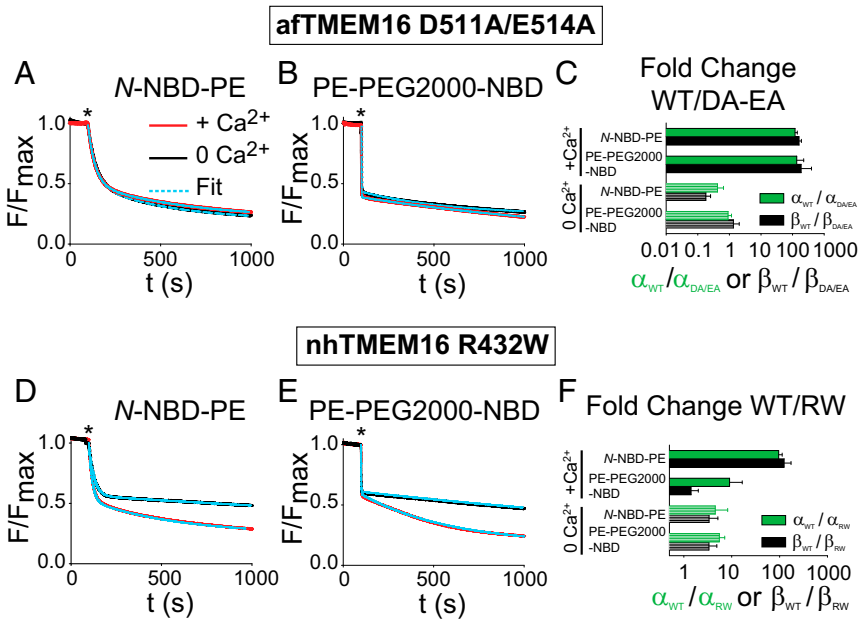

Fig. 3. Phospholipid scrambling of PE-PEG2000-NBD by gating-impaired mutants of TMEM16 scramblases. (*A* and *B*) Representative traces of the time course of the fluorescence reduction in liposomes containing the D511A/E514A mutant of afTMEM16 reconstituted with 0.5 mol % *N*-NBD-PE (*A*) or 0.5 mol % PE-PEG2000-NBD (*B*) in 0.5 mM Ca^{2+} (red) or in 0 mM Ca^{2+} (black). Dashed cyan lines represent fits to Eq. **4**. Asterisk denotes the addition of sodium dithionite. (*C*) Fold change of the forward α (green) and reverse β (black) scrambling rates of *N*-NBD-PE or PE-PEG2000-NBD of the D511A/E514A mutant relative to the WT, in 0.5 mM Ca^{2+} (solid bars) and in the absence of Ca^{2+} (hatched bars). Data are mean ± propagation of the SD. (*D*–*F*) As in *A*–*C* for the R432W mutant of nhTMEM16.

functions as a Ca^{2+}-dependent nonselective ion channel (10, 25, 26, 40). It was also proposed that ion and lipid permeation occur via a shared pathway formed by the groove at the membrane–protein interface (Fig. 1*B*) (41). If the large PEGylated lipids were to permeate through the groove together with the ions, then we expect ion permeation to be blocked or ion selectivity to be affected. We used a flux assay to investigate whether and how the presence of PE-PEG2000 affects ion transport by afTMEM16. In this assay liposomes are prepared in high KCl, the extraliposomal salt is removed, and the total Cl^- trapped inside the vesicles is measured with a Cl^-–sensitive electrode after addition of detergent to solubilize the liposomes (35). Liposomes containing at least one active afTMEM16 channel lose their KCl content, as the nonselective nature of the channel allows the unobstructed passage of both K^+ and Cl^- (10) (Fig. 4*A*). The ∼10–20% fraction of vesicles without an active channel is comparable to the fraction of PF vesicles, f_0, estimated from the scrambling assay (Fig. 1 *E* and *F*). Removal of Ca^{2+} inactivates the channel, reducing the fraction of liposomes containing at least one active channel (Fig. 4*A*). Addition of 0.5 mol % PE-PEG2000 does not affect the activity of the channel in the presence of saturating Ca^{2+} (Fig. 4*A*), or its ion selectivity, as N-methyl-D-glucamine (NMDG) remains poorly permeant through the channel (10) (Fig. 4*B*). The flux assays are end-point measurements of activity and thus lack kinetic resolution. However, if we assume a lower-limit single-channel conductance of $\sim 10^6$ ion s^{-1} for afTMEM16, then it is sufficient for the channels to be open for ∼1% of the time over which the buffer exchange occurs (∼1 s out of ∼100 s) to dissipate the $\sim 10^5$–10^6 ions contained in a liposome. Thus, our results suggest that the permeability of NMDG remains >100-fold lower than that of Na^+ in the presence and absence of the PEGylated lipids. Finally, to rule out the possibility that at low concentrations occupancy of the permeation pathway by the PE-PEG2000 lipids is too low to macroscopically affect ion conduction or selectivity, we increased its concentration 10-fold to 5 mol % and found that neither process is affected (Fig. 4*C*). Taken together these results suggest that while lipid transport can occur outside of the groove, ion transport is likely to be confined to the proteinaceous hemichannel. Finally, the exclusion of NMDG from the permeation pathway suggests that the groove retains its structure during permeation of the PEGylated lipids, and that no major dilation of the pathway is induced by these large substrates.

Concentration Dependence of Scrambling of PEGylated Lipids. The results described above show that afTMEM16 can scramble phospholipids with headgroups much larger than the width of the groove. However, two features of our results remain to be explained. First, why is the initial distribution of the PEG3400/5000 conjugated lipids asymmetric (*SI Appendix*, Fig. S1*E*)? Second, why is the scrambling rate of the lipids conjugated to these larger PEG polymers faster than those of the smaller PEG2000 (Fig. 2*E*)? We considered that the asymmetry in the initial distribution produces an outward-facing concentration gradient of the PEG-conjugated lipids that could account for the

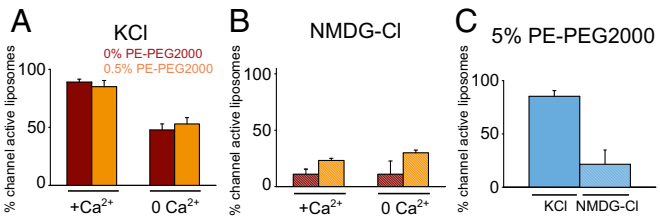

Fig. 4. PE-PEG–conjugated lipids do not alter ion conduction by afTMEM16. (*A* and *B*) Percentage of liposomes containing at least one active and conductive afTMEM16 channel when reconstituted with 300 mM KCl (*A*) or 300 mM NMDG-Cl (*B*), in the absence (dark red) or in the presence of 0.5 mol % PE-PEG2000 lipids (dark yellow), with or without 0.5 mM Ca^{2+}, $n = 5$ in *A* and $n = 3$ in *B*. (*C*) Percentage of liposomes containing at least one active and conductive afTMEM16 channel in the presence of 5 mol % PE-PEG2000 and 0.5 mM Ca^{2+}, $n = 6$.

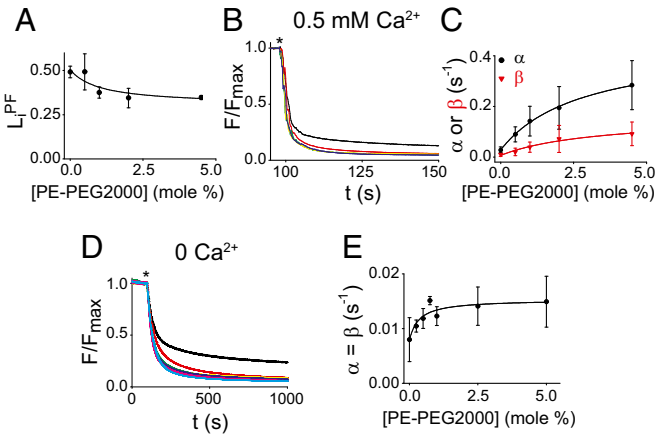

Fig. 5. The effects of PEGylated lipids on phospholipid scrambling are concentration-dependent. (*A*) Fraction of inner-leaflet PE-PEG2000-NBD lipids in protein-free liposomes as a function of [PE-PEG2000]. Solid line represents the fit to a Michaelis–Menten equation with a $K_m^{app} \sim 0.3$ mol %. $n = 6$. (*B*) Time course of fluorescence decay of PE-PEG2000-NBD in afTMEM16-containing liposomes in 0.5 mM Ca^{2+} as a function of the fraction of [PE-PEG2000]. Black, 0.5% PE-PEG2000-NBD (control); red, +0.5% PE-PEG2000; green, +1% PE-PEG2000; yellow, +2% PE-PEG2000; blue, +4.5% PE-PEG2000. (*C*) Scrambling rate constants of PE-PEG2000-NBD, α (black) and β (red), as a function of [PE-PEG2000] with 0.5 mM Ca^{2+}. $n = 6$ (0.5% PE-PEG2000-NBD), 6 (+0.5% PE-PEG2000), 5 (+1%), 6 (+2.5%), and 9 (+4.5%). The line represents the fit to a Michaelis–Menten equation with a $K_m^{app} \sim 3$ mol %. Data points are the mean from $n = 4$–7 experiments from two independent liposome preparations. (*D*) Time course of the fluorescence decay of *N*-NBD-PE afTMEM16-containing liposomes with 0 mM Ca^{2+} as a function of the fraction of reconstituted [PE-PEG2000]. Black, 0.5% *N*-NBD-PE (control); red, +0.25% PE-PEG2000; green, +0.5% PE-PEG2000; yellow, +0.75% PE-PEG2000; blue, +1% PE-PEG2000; pink, +2.5% PE-PEG2000; cyan, +5% PE-PEG2000. (*E*) Scrambling rate constants of *N*-NBD-PE, α and β, as a function of [PE-PEG2000] with 0 mM Ca^{2+}. Average values were obtained by fitting the time courses to Eq. **5** with $\alpha = \beta$. $n = 10$ (0.5% *N*-NBD-PE), $n = 6$ (+0.25% PE-PEG2000), $n = 5$ (+0.5%), $n = 6$ (+0.75%), and $n = 9$ (+1%, +2.5%, +5%). Solid line represents the fit to a Michaelis–Menten equation with a $K_m^{app} \sim 0.3$ mol %. Asterisk in *B* and *D* denotes the addition of sodium dithionite. Data are reported as mean ± SD.

increase in their transport rate. The asymmetry in the distribution could be accounted for by considering that these large, lipid-tethered polymers occupy a nonnegligible fraction of the volume near the inner leaflet of the liposomes and that therefore they might not act as noninteracting particles, but rather that their presence might lead to an excluded volume effect. If this were the case, then we would expect that a similar effect should be seen also for the smaller PE-PEG2000 lipids when reconstituted at higher concentrations. This is indeed the case: The distribution of PE-PEG2000 lipids in PF liposomes becomes progressively more asymmetric as their concentration increases from 0 to 5 mol %, plateauing at $L_i^{PF} \sim 0.35$ (Fig. 5*A*), with $K_m^{app} \sim 0.3$ mol %. We measured the scrambling rate of PE-PEG2000-NBD by afTMEM16 in the presence of varying amounts of PE-PEG2000 (Fig. 5*B*) and found that in the presence of Ca^{2+} the scrambling rate constants α and β increase approximately threefold as the concentration of PE-PEG2000 is raised from 0 to 5 mol % (Fig. 5*C*), with $K_m^{app} \sim 3$ mol %. In the absence of Ca^{2+} the change in rates is difficult to quantify due to the low rate of scrambling of $\sim 10^{-3}$ s^{-1}. These results are consistent with the idea that the distribution and scrambling rates of the large PEG-conjugated lipids are influenced by their concentration, possibly because of an excluded-volume effect.

Normal Phospholipids Can also Be Scrambled Outside the Pathway. We next asked whether an out-of-the-groove mechanism is relevant for lipids with "normal-sized" headgroups. Since scrambling of the large PE-PEG2000 lipids is concentration-dependent (Fig. 5*C*), we reasoned that if normal-sized lipids also can scramble outside the groove, then their rates should display a similar concentration dependence. To test this hypothesis we determined how the scrambling rate of *N*-NBD-PE is affected by varying concentrations of PE-PEG2000. These experiments could only be carried out in the absence of Ca^{2+}, as in saturating Ca^{2+} detection of the scrambling of *N*-NBD-PE is rate-limited by dithionite reduction (Fig. 1 *E* and *F*) (10). As the PE-PEG2000 concentration increases from 0 to 5 mol % scrambling of *N*-NBD-PE becomes progressively faster (Fig. 5*D*) and the scrambling rate constant increases approximately twofold, from ~0.008 to ~0.015 s^{-1} with a $K_m^{app} \sim 0.3$ mol % (Fig. 5*E*). The relatively small increase in the scrambling rate constants likely reflects the fact that the proposed out-of-the-groove scrambling only accounts for a portion of the total lipids being flipped by afTMEM16 and that in the absence of Ca^{2+} lipid transport remains rate-limited by the low spontaneous activity of the groove. Therefore, the scrambling rate of normal phospholipids is affected by the presence of the large PEG-conjugated phospholipids, suggesting that both share a common scrambling mechanism. Thus, small phospholipids also appear to be scrambled outside the cavity-based pathway.

Opsin Scrambles PEG-Conjugated Lipids. Our final goal was to investigate whether scramblases that lack the hydrophilic groove characteristic of the TMEM16s also transport PEG-conjugated phospholipids. The GPCR opsin scrambles lipids (5, 6) with properties that qualitatively resemble those of afTMEM16 in the presence of Ca^{2+} (10). Consistent with past experiments, opsin scrambles *N*-NBD-PE (6) (Fig. 6*A*). The time constant for the exponential decay of *N*-NBD-PE fluorescence on dithionite treatment of opsin-containing liposomes is $\tau_{Ops} \sim 58$ s, similar to that obtained for PF liposomes, $\tau_{PF} \sim 48$ s (Fig. 6*C* and *SI Appendix*, Table S3) and reaches a plateau value $P_{Ops}(PE) \sim 0.32$ (Fig. 6*D* and *SI Appendix*, Table S3). Thus, as observed for afTMEM16, opsin-mediated scrambling of *N*-NBD-PE could not be resolved from the dithionite reduction step. We then tested whether opsin is able to scramble large PEGylated lipids and found that this is the case. When 0.5 mol % PE-PEG2000-NBD is reconstituted, opsin-containing liposomes show fast fluorescence decay (Fig. 6*B*). Similar to our results with afTMEM16, the initial drop in fluorescence occurs more rapidly than for *N*-NBD-PE, with a time constant of ~1.2–1.5 s for both PF liposomes and proteoliposomes (Fig. 6*C* and *SI Appendix*, Table S3). Furthermore, the opsin-containing liposomes reach a plateau value $P_{Ops}(PEG2000) \sim 0.31$ (Fig. 6*D* and *SI Appendix*, Table S3), which is comparable to that of $P_{Ops}(PE)$ (Fig. 6*D* and *SI Appendix*, Table S3). Thus, even with large PEGylated

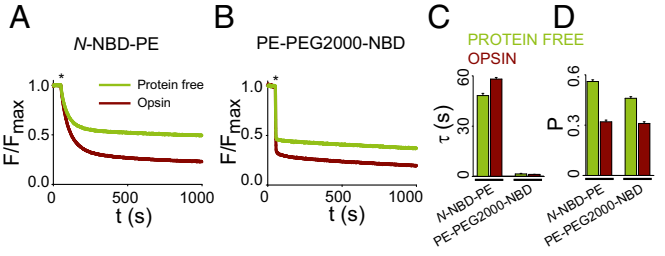

Fig. 6. Phospholipid scrambling of PEG-conjugated lipids by opsin. (*A* and *B*) Representative traces of the time course of the fluorescence reduction in opsin-containing liposomes reconstituted with 0.5 mol % *N*-NBD-PE (*A*) or PE-PEG2000-NBD (*B*). Dashed cyan lines represent fits to Eq. **6**; values of the parameters are reported in *SI Appendix*, Table S3. Asterisk denotes the addition of sodium dithionite. (*C* and *D*) Time constant, τ (*C*) and fluorescence plateau, P (*D*) for PF (green) and opsin-containing liposomes (dark red) derived from fitting the time course of the fluorescence reduction in opsin-containing liposomes with Eq. **6**.

lipids, the rates of scrambling and NBD reduction by dithionite could not be separated, indicating that opsin scrambles these lipids more rapidly than afTMEM16.

Discussion

The membrane-exposed hydrophilic groove of the TMEM16 scramblases suggested that lipid scrambling occurs via a credit-card mechanism in which lipid permeation occurs in a single-file procession, with the headgroup penetrating into the groove while the tails remain in the hydrocarbon core of the membrane (11, 17, 29, 30) (*SI Appendix*, Fig. S7, left subunit). While the involvement of the TMEM16 groove in lipid scrambling has been established both experimentally and computationally (18, 40, 42, 43), it is not clear whether it can account fully for the observed lack of substrate selectivity of these proteins. GPCR scramblases are also relatively unselective and they too appear to use a groove-like lipid translocation pathway, albeit one that is dynamically revealed through conformational rearrangements (16). The lack of substrate specificity of both TMEM16 and GPCR scramblases suggests that there must be a mechanism to scramble lipids that is independent of the specific structural details of the groove.

A readily testable prediction of the credit-card model for scrambling is that the physical dimensions of the groove should impose a defined cutoff on the size of the transported headgroups, as is seen in many ion channels where ions larger than the selectivity filter are excluded and impermeant (44). Lack of such a cutoff would suggest that lipid transport does not necessarily occur through the groove but can also take place outside of the cavity. To test this hypothesis, we measured the scrambling of lipids with headgroups whose dimensions range from 8 to 42 Å, up to approximately four times larger than the width of the groove. We found that both proteins scramble all tested phospholipids, regardless of their headgroup size, with qualitatively similar characteristics. Thus, the membrane-exposed cavity of the TMEM16 scramblases does not impose a size cutoff on the permeating headgroup. To account for these observations, we propose that scramblases also promote transbilayer movement of lipids by locally deforming the membrane (*SI Appendix*, Fig. S7, right subunit). This could be achieved by the introduction of membrane packing defects near the membrane/protein interface, which could reduce the thickness of the membrane and/or facilitate water penetration within the hydrocarbon core. Such deformations are readily reconciled with the credit-card mechanism, as the formation of a single file of lipids whose headgroups penetrate within the slot and span the leaflets is likely to induce defects and distortions of the membrane. Indeed, recent computational work showed that nhTMEM16 thins the membrane by nearly 40% in the proximity of the groove (18) and that lipids hop in and out of the file during transport. This out-of-the-groove mechanism accounts for the low selectivity and high transport rate of most glycerophospholipid scramblases, as lipids permeating outside the groove would not have many strong interactions with the protein hemichannel. Thus, we propose that in the TMEM16 scramblases the groove serves two purposes: It provides a permeation track through which lipid headgroups diffuse in a credit-card mechanism while also bringing the membrane leaflets close together, lowering the energy barrier for lipid transport outside the groove. Indeed, the conformational change that underlies the Ca^{2+}-dependent activation of the TMEM16 scramblases affects transport of all lipids to a similar extent, establishing a clear mechanistic link between these two complementary scrambling mechanisms. Remarkably, impairing opening of the extracellular gate of the lipid pathway via the R432W mutation (39) affects transport of PE more severely than scrambling of a PEGylated lipid, consistent with the idea that translocation of the large headgroup lipids occurs outside the groove.

Our results show that afTMEM16 and opsin scramble both normal and PEG-conjugated lipids very rapidly. The macroscopic rate constants derived from Eq. **5** can be translated into a lipid transport rate under the simplifying assumption that normal and NBD-labeled lipids are transported by afTMEM16 at the same rate. In this case, the lipid transport rate of afTMEM16 can be estimated by considering that a vesicle with average radius ~150 nm (*SI Appendix*, Fig. S1*F*) contains $\sim 5 \times 10^5$ lipids, of which ~2,500 are labeled, and approximately five copies of the afTMEM16 dimer (10). Thus, the scrambling rate constant measured in saturating Ca^{2+}, $\alpha(\text{PE}, +Ca^{2+}) > 0.2\ s^{-1}$, corresponds to a lipid transport rate $>2 \times 10^4$ lipid s^{-1}, a value that drops to ~100 lipid s^{-1} in the absence of Ca^{2+}. Surprisingly, our data suggest afTMEM16 transports PE-PEG2000 at rates that are comparable to those of PE lipids $\sim 10^4$ and 100 lipids s^{-1}, in the presence and absence of Ca^{2+}, respectively. Further, opsin appears to scramble PE-PEG2000 faster than our detection limit, imposing a lower bound limit on its transport rate of $>10^5$ lipid s^{-1}, a rate that is even faster than that of afTMEM16. It is important to consider the simplifying assumptions we made in this analysis. First, we considered a uniform distribution of the scramblases across liposomes of uniform size, an unrealistic assumption given the relatively broad size distribution of the vesicles (*SI Appendix*, Fig. S1*F*). Second, to minimize the number of free parameters in our fits we constrained $\alpha = \beta$ in saturating Ca^{2+} (*SI Appendix*, Table S1). However, it is possible that afTMEM16 scrambles lipids with rates that are unequal in the two directions and/or that the protein has a preferred direction of incorporation in vesicles. Both of these factors could lead to an asymmetry in the macroscopic rate constants. Indeed, in zero Ca^{2+} we do see a small asymmetry in the rates of transport, with $\alpha > \beta$ (*SI Appendix*, Table S1). Finally, the relationship between the macroscopic rate constant and unitary transport rate is not linear in a regime where liposomes are populated by multiple copies of the protein (35), leading to an underestimation of the unitary rate. Despite these limitations, our experiments and analysis provide a quantitative measurement of the unitary rates of lipid transport of the TMEM16 scramblases and can serve to quantitatively assess the effects of mutants as well as being generalized to other systems.

Our data suggest that while lipid movement can occur both within and outside the groove, ion transport is more constrained and likely only takes place within the hemichannel provided by the hydrophilic cavity. Indeed, while afTMEM16 allows for passage of lipid-conjugated molecules as large as PEG5000 (radius ~40 Å), it excludes the much smaller NMDG ion (radius ~4.5 Å) (Fig. 4*A*) (10). Importantly, the exclusion of NMDG from the pore is not affected by the presence of the large PEG molecules (Fig. 4*A*), indicating that these compounds do not "punch holes" in the membrane while being scrambled and that the groove does not dilate to accommodate them. One possible consideration is that the PEGs used here are flexible polymers, and therefore it could be that their permeation occurs in an unwound state, as a chain rather than a globule. Indeed, our DLS measurements only capture the average size of the PEGs in solution but extensive theoretical and simulation work indicates that these molecules can adopt a variety of sizes and shapes (45–47). While it is unlikely that the PEGs move across the membrane as a sphere of 25–42 Å, two pieces of evidence suggest that they do not permeate as long extended chains. First, the measured scrambling rate of the NBD-PEGylated lipids is comparable to that of the much smaller PE lipids, both in the presence and absence of Ca^{2+} (Fig. 2 *E* and *F*). If the polymers had to unwind to get through the groove, their permeation rate should be much slower than that of the smaller lipids, as their passage time should increase with the square root of their length. Indeed, if this were the case then we would expect the PEG-conjugated lipids to function as permeant blockers of the scramblases. Rather, we find that increasing the concentration of PE-PEG2000 increases the transport rate of the normal lipids (Fig. 5 *D* and *E*), indicating

that the two lipids share a pathway through which permeation is not competitive. Second, if the PEG molecules uncoiled during permeation then we would expect that the larger PEGs should take longer to permeate, as the square root of their length will progressively increase. In contrast, we find that PE-PEG3400-NBD and PE-PEG5000-NBD permeate faster than the smaller PE-PEG2000-NBD (Fig. 2 *A*–*C* and *E*). An alternative possibility is that the NBD fluorophore moves through the groove without the headgroup and the rest of the PEG molecule crossing the membrane. In this scenario, the PEG chain would be expected to have long dwell-time occupancy of the permeation pathway, as its NBD-labeled end would need to first diffuse through the groove to traverse the membrane and then diffuse back—as the forward and reverse scrambling rates of the PEGylated lipids are comparable (*SI Appendix*, Table S1). In this case, the PEGylated lipids should act as permeant blockers, as occupancy of the pathway by the PEG polymer chain would sterically prevent permeation of the normal PE lipids. In contrast, we found that increasing the PE-PEG concentration leads to faster scrambling for both PE-PEG (Fig. 5 *B* and *C*) and normal PE lipids (Fig. 5 *D* and *E*). This is consistent with the idea that both lipids permeate through a shared mechanism and suggests that the residence time of the PEG chains through the groove is comparable to that of regular lipids. These results thus suggest that while it is unlikely that the PEG molecules permeate as 25–42 Å spheres, it is likely that they do so while retaining some of their globular structure.

In conclusion, our findings suggest that scrambling mediated by TMEM16 proteins and GPCRs occurs through dual mechanisms: Lipids can traverse the membrane either by passing through a hydrophilic groove formed by the protein, or outside this cavity due to the presence of local defects in the packing of the membrane that depends on the conformational rearrangements associated with the opening of the groove. This dual mechanism accounts well for the observed properties of these scramblases and explains how these proteins share many functional characteristics while bearing no structural resemblance. We propose that this mechanism may be a general feature of other scramblases and that it contributes to their physiological task of moving lipids of various charge, size, and shapes across biological membranes.

Materials and Methods

Protein Expression and Purification. Expression and purification of afTMEM16 were carried out as previously described (10). Briefly, the uracil-selectable pDDGFP2 vector containing the afTMEM16-His8 gene was transformed into *Saccharomyces cerevisiae* FYG217 [MAT*a*, *ura*3–52, *lys*2Δ201, *pep*4Δ (48, 49)] competent cells carrying a URA3 deletion for positive selection. Cells were grown in yeast synthetic drop-out medium supplemented with uracil (CSM-URA; MP Biomedicals). Expression was induced with 2% (wt/vol) galactose at 30 °C. Cells were collected after 22 h and lysed in an EmulsiFlex-C5 homogenizer at 25,000 psi in buffer P [150 mM KCl, 10% (wt/vol) glycerol, and 50 mM Tris·HCl, pH 8]. Extraction was carried out in the presence of 1% (wt/vol) digitonin (Millipore Sigma). afTMEM16 was purified via Ni-NTA agarose resin (Qiagen) and Superdex 200 column (GE Healthcare) with buffer P containing 0.12% (wt/vol) digitonin. The 8-His-tag was cleaved by overnight treatment with tobacco etch virus protease before running the protein onto the size-exclusion column. Expression and purification of WT and mutant C-terminal Myc-streptavidin-binding peptide-tagged nhTMEM16 constructs (11) were carried out as described. Briefly, *S. cerevisiae* cells (FGY217) were transformed and grown to an OD of 0.8 and protein expression was induced by the addition of 2% galactose for 40 h at 25 °C. Cells were resuspended in lysis buffer (150 mM NaCl and 50 mM Hepes, pH 7.6) containing protease inhibitor mixture and lysed with an EmulsiFlex-C3 homogenizer at pressures above 25,000 psi. Membrane proteins were extracted by supplementing the lysis buffer with 2% *n*-dodecyl-β-D-maltopyranoside (DDM; Anatrace) and incubated for 1.5 h at 4 °C. Proteins were purified using Streptavidin Plus UltraLink Resin (Thermo Fisher Scientific) followed by gel filtration chromatography with buffer (150 mM NaCl, 5 mM Hepes, pH 7.6, and 0.025% DDM) by using a Superdex 200 column (GE Healthcare). Opsin was prepared as described previously (5). Briefly, C-terminally FLAG-tagged thermostable (N2C/D282C) bovine opsin was expressed in HEK293S GnTI$^-$ cells (50), purified by FLAG affinity chromatography, and quantified by Coomassie staining after SDS/PAGE, using an in-gel BSA standard. Cells were obtained from Daniel Oprian, Brandeis University, Waltham, MA, and were not further authenticated, although the glycosylation status of expressed opsin was consistent with the GnTI defect in the cells.

NBD-Labeled PEG-Conjugated Phospholipid Synthesis (NBD-PE-PEG Lipids). DSPE-PEG2000 (1,2-distearoyl-*sn*-glycero-3-phosphoethanolamine-*N*-[amino (polyethylene glycol)-2000]; Avanti Polar Lipids), DSPE-PEG3400, and DSPE-PEG5000 (Nanocs) were converted to fluorescently labeled NBD conjugates by reaction with succinimidyl 6-(*N*-(7-nitrobenz-2-oxa-1,3-diazol-4-yl)amino) hexanoate as follows. DSPE-PEG amine (9.8 mg, 0.0035 mmol) was dissolved in anhydrous CH_2Cl_2 (1.5 mL). Triethylamine (0.01 mL) was added, followed by succinimidyl 6-(*N*-(7-nitrobenz-2-oxa-1,3-diazol-4-yl)amino) hexanoate (2.7 mg, 0.0070 mmol). The reaction mixture was stirred for 2 h under N_2. Reaction progress was monitored by TLC on silica gel 60 plates using $CHCl_3/CH_3OH$ (85:15, vol/vol). The crude reaction mixture was dried under N_2 and the product was purified by preparative TLC on silica using the same solvent system. The band corresponding to the product was scraped from the TLC plate and collected using a fritted glass funnel with a glass wool plug. The product was eluted with 50% $CHCl_3/CH_3OH$ using vacuum filtration. The purified DSPE-PEG-NBD conjugates were verified by TLC and MALDI-TOF mass spectrometry. MALDI-TOF analysis revealed an envelope of masses for each lipid, with prominent peaks corresponding to 3,053, 4,440, and 6,052 Da for PE-PEG2000-NBD, PE-PEG3400-NBD, and PE-PEG5000-NBD, respectively.

Liposome Preparation. Liposomes were formed in *Escherichia coli* polar extract for the experiments with afTMEM16 and in a 2.25:0.75:1 mixture of 1-palmitoyl-2-oleoyl-*sn*-glycero-3-phosphoethanolamine:1-palmitoyl-2-oleoyl-*sn*-glycero-3-phospho-(1′-*rac*-glycerol) (POPG):L-α-phosphatidylcholine (egg, chicken 60%) for the experiments with nhTMEM16 (all lipids from Avanti Polar Lipids). Unless otherwise stated, lipids (20 mg/mL) were dissolved in buffer L (300 mM KCl and 50 mM Hepes, pH 7.4) and 35 mM CHAPS (Thermo Fisher Scientific). The desired amount (mole percent) of NBD-PE, PE-PEGX-NBD lipids, or PE-PEGX lipids (Avanti Polar Lipid, Nanocs) was included before dissolving the lipids. Unless otherwise noted, 0.5 mol % of NBD lipids were used. Purified proteins were added to the detergent/lipid suspension to a final 5 μg protein/mg lipid ratio. Detergent was removed by Bio-Beads SM-2 (Bio-Rad) treatment: four changes of 200 mg Bio-Beads/mL of liposomes preequilibrated with buffer L and incubated at 4 °C with gentle rotation for 24 h. Liposomes were collected, flash-frozen in liquid nitrogen, and stored at −80 °C. Then, 0.5 mM $Ca(NO_3)_2$ or 10 mM EGTA was added by three to five freeze/thaw cycles before performing the experiments. One of the main sources of variability among different liposome batches is the total amount of lipid recovered during resuspension and detergent removal. Therefore, to facilitate the comparison of scrambling and flux data obtained from different liposome preparations the following steps were taken. First, the same batch of freshly resuspended lipids was used for all samples in each experimental set. Second, liposomes utilized in experiments entailing the change of a single parameter (i.e., the PE-PEG2000 titrations in Fig. 5 or the PF reconstitutions in different PE-PEGylated lipids in *SI Appendix*, Fig. S1) were prepared simultaneously. Third, liposomes were extruded immediately before their use. Opsin was reconstituted by a detergent destabilization procedure as described (5, 51, 52) using preformed vesicles consisting of a 9:1 (mol:mol) mixture of 2-Oleoyl-1-palmitoyl-sn-glycero-3-phosphocholine (POPC) and POPG.

Scrambling Assay. Scrambling measurements were performed as previously described (10). The fluorescence intensity (excitation 470 nm, emission 530 nm) was recorded in a PTI spectrofluorimeter. Liposomes were formed via extrusion through a 400-nm membrane. Twenty microliters of the liposome suspension was diluted into 2 mL of external solution containing 300 mM KCl, 50 mM Hepes, and 0.5 mM $Ca(NO_3)_2$ or 10 mM EGTA, pH 7.4, in a stirred cuvette at 23 °C. Sodium dithionite (40 μL of a 1 M stock solution prepared in 0.5 M Tris·HCl, pH 10; 20 mM final concentration) was added after 100 s to the cuvette to start the reaction. Data were collected using FelixGX 4.1.0 at a sampling rate of 10 Hz.

Quantification of Scrambling Activity. The total fluorescence of a population of afTMEM16-containing proteoliposomes reconstituted with NBD-labeled lipids is the sum of the signal from vesicles that contain at least one active scramblase, $F_{Scr}(t)$, and of those that are empty, $F_{PF}(t)$, weighted by their relative abundance:

$$F_{tot}(t) = f_0 F_{PF}(t) + (1 - f_0) F_{Scr}(t), \quad [1]$$

where f_0 is the fraction of empty vesicles. The fluorescence signal, F(t), is proportional to the sum of the signal from fluorescent lipids in the inner, $L_i(t)$, and outer leaflets, $L_o(t)$, so that

$$F(t) = L_i(t) + L_o(t).$$

In PF vesicles only lipids in the outer leaflet are accessible to dithionite, so that the time course of fluorescence decay is described by the following scheme:

$$L_i^{PF} \quad L_o \xrightarrow{\gamma} L^*, \quad \text{(Scheme 1)}$$

where L^* is the bleached, nonfluorescent form of the NBD-labeled lipids after dithionite reduction, and the dithionite reduction rate constant $\gamma = \gamma'[D]$, where γ' is the second-order rate constant of dithionite reduction and [D] is the dithionite concentration. Note that the L_i-to-L_o transition can be ignored as there are no scramblases. Therefore, $F_{PF}(t)$ will be given by

$$F_{PF}(t) = \left(L_i^{PF} + \left(1 - L_i^{PF}\right) e^{-\gamma t}\right). \quad [2]$$

The time course of fluorescence decay following dithionite addition to a suspension of liposomes containing at least one active scramblase is described by a three-state Markov model (Fig. 1*D*) (36),

$$L_i \underset{\beta}{\overset{\alpha}{\rightleftarrows}} L_o \xrightarrow{\gamma} L^*, \quad \text{(Scheme 2)}$$

where α and β are the forward and reverse scrambling rate constants. The time evolution of this system can be analytically derived (*SI Appendix, Appendix 1*) and, under the additional assumption that at $t = 0$ the system is at the equilibrium state generated by the scramblases, is given by

$$F_{Scr}(t) = \frac{\left\{\alpha(\lambda_2 + \gamma)(\lambda_1 + \alpha + \beta) e^{\lambda_1 t} + \lambda_1 \beta(\lambda_2 + \alpha + \beta + \gamma) e^{\lambda_2 t}\right\}}{D(\alpha + \beta)} \quad [3]$$

With

$$\lambda_1 = -\frac{(\alpha + \beta + \gamma) - \sqrt{(\alpha + \beta + \gamma)^2 - 4\alpha\gamma}}{2}$$

$$\lambda_2 = -\frac{(\alpha + \beta + \gamma) + \sqrt{(\alpha + \beta + \gamma)^2 - 4\alpha\gamma}}{2}$$

and

$$D = (\lambda_1 + \alpha)(\lambda_2 + \beta + \gamma) - \alpha\beta.$$

Substituting Eqs. **2** and **3** into Eq. **1** we get the time evolution of the total system:

$$F_{tot}(t) = f_0\left(L_i^{PF} + \left(1 - L_i^{PF}\right) e^{-\gamma t}\right) + \frac{(1 - f_0)}{D(\alpha + \beta)}\left\{\alpha(\lambda_2 + \gamma)(\lambda_1 + \alpha + \beta) e^{\lambda_1 t} + \lambda_1 \beta(\lambda_2 + \alpha + \beta + \gamma) e^{\lambda_2 t}\right\}. \quad [4]$$

Under the simplifying assumption that the forward and reverse rates of scrambling are identical and that in PF liposomes the lipids distribute equally in the two leaflets, $\alpha = \beta$ and $L_i^{PF} = L_o^{PF} = 0.5$, the time evolution of the signal becomes

$$F_{tot}(t) = \frac{f_0}{2}\left(1 + e^{-\gamma t}\right) + \frac{(1 - f_0)}{2D}\left[(\lambda_2 + \gamma)(\lambda_1 + 2\alpha) e^{\lambda_1 t} + \lambda_1(\lambda_2 + 2\alpha + \gamma) e^{\lambda_2 t}\right]. \quad [5]$$

See *SI Appendix, Appendix 1* for a complete derivation of Eqs. **3**–**5** and the assumptions made. In some traces obtained with PF vesicles an additional slow decrease in fluorescence was evident, which reflects a combination of the rate of dithionite entry into the vesicles and spontaneous flipping of lipids. However, in all cases this component was >100-fold smaller than the slowest measured rate constant and was therefore neglected from the analysis (*SI Appendix*, Tables S1 and S3).

In the case of opsin-containing liposomes it was not possible to separate scrambling from the dithionite chemical reaction. Therefore, the time course of the fluorescence decay was fit to a single exponential function with the addition of a linear component that represents a slow process (as above, due to a combination of dithionite entry and spontaneous scrambling) present in all traces (51):

$$F/F_{max} = (1 - P) e^{\frac{-t}{\tau}} + P - Lt, \quad [6]$$

where P is the fluorescence plateau value and L is the slope of the linear component. Values are reported in *SI Appendix*, Table S3 and shown in Fig. 6 *C* and *D*.

DLS. DLS was used to evaluate the size of the headgroups of PEGylated lipids and also the diameter of liposomes. For analysis of headgroups, PE-PEGX-NBD lipids were deacylated by methanolysis under basic conditions (34) as follows. At least 1 mg of PE-PEGX-NBD was dissolved in methanol (0.9 mL) and transferred to a glass tube. Upon addition of 10.0 M NaOH (0.1 mL) the sample was incubated at 60 °C for 3–4 h (without stirring), dried under nitrogen, resuspended in chloroform, and applied to a preparative silica TLC plate. The plate was developed using chloroform/methanol 8:2 (vol/vol) and silica corresponding to the band of interest was scraped and collected into a fritted glass funnel. The deacylated product was eluted with 1:1 chloroform/methanol (vol/vol) using vacuum filtration and transferred to a tared round-bottomed flask. The product was dried and dissolved in methanol to make a 1 mg/mL solution. After clarification by microcentrifugation (15 min, 6,000 × *g*, 4 °C) the sample was analyzed by DLS (Zetasizer Nano-S; Malvern Instruments) at 25 °C with 0-s delay using a dust-free quartz cuvette. For analysis of liposomes, samples were extruded through a 400-nm filter immediately before DLS measurements to match the way samples are prepared for functional assays. Measurements were obtained in $n = 3$ independent experiments from $n = 2$ biological replicates. The averaged size distribution was fit to a log normal distribution of the form

$$P(D) = Ae^{-0.5\left(\frac{\ln\frac{D}{D_0}}{b}\right)^2}, \quad [7]$$

where A is the amplitude, D_0 is the median diameter, and b is the shape of the lognormal distribution. From these the mean and variance of the distributions were determined as

$$D = D_0 e^{0.5b^2} \text{ and } \sigma = \sqrt{{D_0}^2 e^{b^2}\left(e^{b^2} - 1\right)}. \quad [8]$$

Flux Assay. Liposomes prepared in buffer L were extruded through a 400-nm membrane filter and passed through a Sephadex G-50 column (Sigma-Aldrich) preequilibrated in the desired external buffer [1 mM KCl or 1 mM NMDG-Cl, 300 Sorbitol, 50 mM Hepes, pH 7.4, and 0.5 mM $Ca(NO_3)_2$]. Two hundred microliters of liposomes were diluted into 1.8 mL of buffer and the time course of Cl^- release was monitored with an AgCl electrode. The experiment was terminated after 90 s by addition of 40 μL of 1.5 M *n*-octyl-β-D-glucopyranoside (Affymetrix) to dissolve liposomes and determine the total Cl^- content of the liposomes, ΔCl^-. To minimize the variability, for each set of experiments liposomes were prepared the same day using the same batch of lipids. ΔCl^- was normalized to the average Cl^- content of PF liposomes in the presence of 0.5 mM Ca^{2+} from the same day.

Cryoelectron Microscopy. Extruded liposomes (3.5 μL) were applied to glow-discharged 400-mesh copper C-flat R2/2 holey carbon grids. Grids were manually blotted and the sample addition was repeated. After a 2-min incubation following the second sample addition, grids were blotted for 3 s under 100% humidity and flash-frozen in liquid ethane cooled by liquid nitrogen using a Vitrobot Mark IV (FEI). Cryoelectron microscopy data were collected on a 120-kV Technai T12 BioTWIN microscope using the Leginon data collection software (53) and a TVIPS F416 CMOS detector with an exposure time of 0.8 s and a defocus of −3 μM. Liposome diameters were measured using the ImageJ software (NIH) and their distribution was fit to a lognormal distribution (Eqs. **7** and **8**).

Data Analysis and Statistics. Data were analyzed using the Ana software (M. Pusch, Istituto di Biofisica, Genova, Italy) and SigmaPlot 10.0. The experiments were repeated at least three times; exact numbers are reported in the text or in the figure legends. Unless otherwise specified, all data are reported as mean ± SEM or mean ± SD.

ACKNOWLEDGMENTS. We thank members of the A.A. lab for support and discussion, Prof. Ching Tung for use of a DLS instrument, and Milica Tešić Mark (Proteomics Resource Center, The Rockefeller University) for assistance with MALDI-TOF mass spectrometry. This work was supported by NIH Grant GM106717 (to A.A. and A.K.M.), an Irma T. Hirschl/Monique Weill-Caulier Scholar Award (to A.A.), NIH Grant EY028314 (to A.K.M.), and Velux Stiftung Grant Project 881 (to A.K.M.). Some of this work was performed at the Simons Electron Microscopy Center and National Resource

for Automated Molecular Microscopy located at the New York Structural Biology Center, supported by grants from the Simons Foundation (349247), Empire State Development's Division of Science, Technology and Innovation, and the NIH National Institute of General Medical Sciences (GM103310) with additional support from Agouron Institute (F00316) and NIH Grant S10 OD019994-01.

1. Balasubramanian K, Schroit AJ (2003) Aminophospholipid asymmetry: A matter of life and death. *Annu Rev Physiol* 65:701–734.
2. Bevers EM, Williamson PL (2010) Phospholipid scramblase: An update. *FEBS Lett* 584: 2724–2730.
3. Segawa K, Suzuki J, Nagata S (2011) Constitutive exposure of phosphatidylserine on viable cells. *Proc Natl Acad Sci USA* 108:19246–19251.
4. Griffin DA, et al. (2016) Defective membrane fusion and repair in Anoctamin5-deficient muscular dystrophy. *Hum Mol Genet* 25:1900–1911.
5. Goren MA, et al. (2014) Constitutive phospholipid scramblase activity of a G protein-coupled receptor. *Nat Commun* 5:5115.
6. Menon I, et al. (2011) Opsin is a phospholipid flippase. *Curr Biol* 21:149–153.
7. Nagata S, Suzuki J, Segawa K, Fujii T (2016) Exposure of phosphatidylserine on the cell surface. *Cell Death Differ* 23:952–961.
8. Suzuki J, Imanishi E, Nagata S (2016) Xkr8 phospholipid scrambling complex in apoptotic phosphatidylserine exposure. *Proc Natl Acad Sci USA* 113:9509–9514.
9. Suzuki J, Umeda M, Sims PJ, Nagata S (2010) Calcium-dependent phospholipid scrambling by TMEM16F. *Nature* 468:834–838.
10. Malvezzi M, et al. (2013) Ca2+-dependent phospholipid scrambling by a reconstituted TMEM16 ion channel. *Nat Commun* 4:2367.
11. Brunner JD, Lim NK, Schenck S, Duerst A, Dutzler R (2014) X-ray structure of a calcium-activated TMEM16 lipid scramblase. *Nature* 516:207–212.
12. Suzuki J, Denning DP, Imanishi E, Horvitz HR, Nagata S (2013) Xk-related protein 8 and CED-8 promote phosphatidylserine exposure in apoptotic cells. *Science* 341: 403–406.
13. Ernst OP, Menon AK (2015) Phospholipid scrambling by rhodopsin. *Photochem Photobiol Sci* 14:1922–1931.
14. Suzuki J, Imanishi E, Nagata S (2014) Exposure of phosphatidylserine by Xk-related protein family members during apoptosis. *J Biol Chem* 289:30257–30267.
15. Pandey K, et al. (2017) An engineered opsin monomer scrambles phospholipids. *Sci Rep* 7:16741.
16. Morra G, et al. (2018) Mechanisms of lipid scrambling by the G protein-coupled receptor opsin. *Structure* 26:356–367.e3.
17. Brunner JD, Schenck S, Dutzler R (2016) Structural basis for phospholipid scrambling in the TMEM16 family. *Curr Opin Struct Biol* 39:61–70.
18. Bethel NP, Grabe M (2016) Atomistic insight into lipid translocation by a TMEM16 scramblase. *Proc Natl Acad Sci USA* 113:14049–14054.
19. Whitlock JM, Hartzell HC (2017) Anoctamins/TMEM16 proteins: Chloride channels flirting with lipids and extracellular vesicles. *Annu Rev Physiol* 79:119–143.
20. Yang YD, et al. (2008) TMEM16A confers receptor-activated calcium-dependent chloride conductance. *Nature* 455:1210–1215.
21. Schroeder BC, Cheng T, Jan YN, Jan LY (2008) Expression cloning of TMEM16A as a calcium-activated chloride channel subunit. *Cell* 134:1019–1029.
22. Caputo A, et al. (2008) TMEM16A, a membrane protein associated with calcium-dependent chloride channel activity. *Science* 322:590–594.
23. Terashima H, Picollo A, Accardi A (2013) Purified TMEM16A is sufficient to form Ca2+-activated Cl- channels. *Proc Natl Acad Sci USA* 110:19354–19359.
24. Yang H, et al. (2012) TMEM16F forms a Ca2+-activated cation channel required for lipid scrambling in platelets during blood coagulation. *Cell* 151:111–122.
25. Lee BC, Menon AK, Accardi A (2016) The nhTMEM16 scramblase is also a nonselective ion channel. *Biophys J* 111:1919–1924.
26. Scudieri P, et al. (2015) Ion channel and lipid scramblase activity associated with expression of TMEM16F/ANO6 isoforms. *J Physiol* 593:3829–3848.
27. Yu K, et al. (2015) Identification of a lipid scrambling domain in ANO6/TMEM16F. *elife* 4:e06901.
28. Gyobu S, et al. (2015) A role of TMEM16E carrying a scrambling domain in sperm motility. *Mol Cell Biol* 36:645–659.
29. Pomorski T, Menon AK (2006) Lipid flippases and their biological functions. *Cell Mol Life Sci* 63:2908–2921.
30. Pomorski TG, Menon AK (2016) Lipid somersaults: Uncovering the mechanisms of protein-mediated lipid flipping. *Prog Lipid Res* 64:69–84.
31. Dekkers DW, Comfurius P, Bevers EM, Zwaal RF (2002) Comparison between Ca2+-induced scrambling of various fluorescently labelled lipid analogues in red blood cells. *Biochem J* 362:741–747.
32. Paulino C, et al. (2017) Structural basis for anion conduction in the calcium-activated chloride channel TMEM16A. *eLife* 6:1–23.
33. Jiang T, Yu K, Hartzell HC, Tajkhorshid E (2017) Lipids and ions traverse the membrane by the same physical pathway in the nhTMEM16 scramblase. *eLife* 6:e28671.
34. Hanahan DJ (1997) *A Guide to Phospholipid Chemistry* (Oxford Univ Press, Oxford, England), p 71.
35. Walden M, et al. (2007) Uncoupling and turnover in a Cl^-/H^+ exchange transporter. *J Gen Physiol* 129:317–329.
36. Marx U, et al. (2000) Rapid flip-flop of phospholipids in endoplasmic reticulum membranes studied by a stopped-flow approach. *Biophys J* 78:2628–2640.
37. Paulino C, Kalienkova V, Lam AKM, Neldner Y, Dutzler R (2017) Activation mechanism of the calcium-activated chloride channel TMEM16A revealed by cryo-EM. *Nature* 552:421–425.
38. Dang S, et al. (2017) Cryo-EM structures of the TMEM16A calcium-activated chloride channel. *Nature* 552:426–429.
39. Lee BC, et al., Gating mechanism of the lipid pathway in a TMEM16 scramblase. *Nat Comms*, in press.
40. Yu K, et al. (2015) Identification of a lipid scrambling domain in ANO6/TMEM16F. *eLife* 4:e06901.
41. Whitlock JM, Hartzell HC (2016) A pore idea: The ion conduction pathway of TMEM16/ANO proteins is composed partly of lipid. *Pflugers Arch* 468:455–473.
42. Suzuki T, Suzuki J, Nagata S (2014) Functional swapping between transmembrane proteins TMEM16A and TMEM16F. *J Biol Chem* 289:7438–7447.
43. Gyobu S, Ishihara K, Suzuki J, Segawa K, Nagata S (2017) Characterization of the scrambling domain of the TMEM16 family. *Proc Natl Acad Sci USA* 114:6274–6279.
44. Hille B, Schwarz W (1978) Potassium channels as multi-ion single-file pores. *J Gen Physiol* 72:409–442.
45. Kenworthy AK, Hristova K, Needham D, McIntosh TJ (1995) Range and magnitude of the steric pressure between bilayers containing phospholipids with covalently attached poly(ethylene glycol). *Biophys J* 68:1921–1936.
46. Nicholas AR, Scott MJ, Kennedy NI, Jones MN (2000) Effect of grafted polyethylene glycol (PEG) on the size, encapsulation efficiency and permeability of vesicles. *Biochim Biophys Acta* 1463:167–178.
47. Nikolova AN, Jones MN (1996) Effect of grafted PEG-2000 on the size and permeability of vesicles. *Biochim Biophys Acta* 1304:120–128.
48. Kota J, Melin-Larsson M, Ljungdahl PO, Forsberg H (2007) Ssh4, Rcr2 and Rcr1 affect plasma membrane transporter activity in Saccharomyces cerevisiae. *Genetics* 175: 1681–1694.
49. Drew D, et al. (2008) GFP-based optimization scheme for the overexpression and purification of eukaryotic membrane proteins in Saccharomyces cerevisiae. *Nat Protoc* 3:784–798.
50. Reeves PJ, Callewaert N, Contreras R, Khorana HG (2002) Structure and function in rhodopsin: High-level expression of rhodopsin with restricted and homogeneous N-glycosylation by a tetracycline-inducible N-acetylglucosaminyltransferase I-negative HEK293S stable mammalian cell line. *Proc Natl Acad Sci USA* 99:13419–13424.
51. Ploier B, et al. (2016) Dimerization deficiency of enigmatic retinitis pigmentosa-linked rhodopsin mutants. *Nat Commun* 7:12832.
52. Ploier B, Menon AK (2016) A fluorescence-based assay of phospholipid scramblase activity. *J Vis Exp*, 10.3791/54635.
53. Suloway C, et al. (2005) Automated molecular microscopy: The new Leginon system. *J Struct Biol* 151:41–60.

Supplementary Material

Supplementary Figure 1. Generation, characterization and vesicle reconstitution of PE-PEG-NBD lipids

A) Chemical structures of NBD phospholipids used in this study. 1-myristoyl-2-{6-[(7-nitro-2-1,3-benzoxadiazol-4-yl)amino]hexanoyl}-*sn*-glycero-3-phosphoethanolamine, C_6-NBD-PE; 1,2-dipalmitoyl-*sn*-glycero-3-phosphoethanolamine-N-(7-nitro-2-1,3-benzoxadiazol-4-yl), *N*-NBD-PE; 1,2-distearoyl-sn-glycero-3-phosphoethanolamine-N-[amino(polyethylene glycol)-X], PE-PEG X-NBD (X = 2000, 3400 or 5000, *see Methods*). B) Dynamic light scattering of PEG2000 (blue), PEG3400 (cyan) and PEG5000 (dark green) isolated from PE lipids by methanolysis under basic conditions (*see Methods*). The average diameters are 25Å for PEG2000, 35Å for PEG3400 and 42Å for PEG5000. Each point (circle) represents the average of 6 experiments. The reported size distribution was fit to a Gaussian function to determine the average size. C) Representative traces of the dithionite reduction of NBD fluorophores conjugated to glucose at 0.5 mole% (dashed black line) or to the following lipids and reconstituted in protein-free liposomes at 0.5 mole%: C_6-NBD-PE (orange), *N*-NBD-PE (red), PE-PEG2000-NBD (blue), PE-PEG3400-NBD (cyan), PE-PEG5000-NBD (dark green). All experiments were carried out in the presence of 0.5mM Ca^{2+}. (*) denotes the addition of 20 mM sodium dithionite. D) NBD reduction rate constant, γ, for NBD-glucose (black, n=3), C_6-NBD-PE (orange, n=23), *N*-NBD-PE (red, n=11), PE-PEG2000-NBD (blue, n=22), PE-PEG3400-NBD (cyan, n=8), PE-PEG5000-NBD (dark green, n=9). In each case γ was determined by fitting the fluorescence time courses to Eq. 2. Values are reported in Table 1. E) Average normalized steady-state fluorescence (L_i^{PF}) of protein-free liposomes containing NBD-lipids. F) Dynamic light scattering profiles of protein-free liposomes containing no PEGylated lipids (Control, red), 0.5 mole % PE-PEG2000 (blue), 0.5% PE-PEG3400 (cyan), 0.5% PE-PEG5000 (dark green) or 5% PE-PEG2000 (grey). Each point (circle) represents the average of n=6 independent experiments from N=2 biological preparations. Error bars are the S.D. Solid lines represent the fits of the data to a log-normal distribution (Eq. 7). The mean (<D>) and variance (σ) of the distribution in each condition are reported in Suppl. Fig. 4C. G) Total Cl^- content of protein-free liposomes, with 0.5mM Ca^{2+}, without PEGylated lipids (red, n=8), with 0.5 mole% PE-PEG2000 (blue, n=8), PE-PEG3400 (cyan, n=8) or PE-PEG5000 (dark green, n=8), 5 mole% PE-PEG2000 (grey, n=13) measured upon dissolving the liposomes with 1.5M β-OctylGlucoside (1).

* denotes that the difference with the control is not statistically significant ($p>0.05$). Data is mean ± S.D. from at least three independent preparations.

Supplementary Figure 2. Characterization of PE-PEG-conjugated lipids

A) Thin layer chromatography (TLC) of PE-PEG2000-NBD, PE-PEG3400 NBD and PE-PEG5000. TLC plates were developed in 85% $CHCl_3$:MeOH (v/v). The solvent-front is at the top of the plate. B) MALDI-TOF analysis of PE-PEGylated-NBD lipids comparing the expected mass and the experimental data for each lipid. The values for the peak and its corresponding full width at half maximum (FWHM) are reported.

Supplementary Figure 3. Cryo-electron microscopy of liposomes reconstituted with PE-PEG-conjugated lipids

A) Representative images of protein-free liposomes containing no PEGylated lipids (control), 0.5% PE-PEG2000/PEG3400/PEG5000 or 5% PE-PEG2000. Scale bar for each panel is 200 nm. Total vesicle numbers (N_V) and image count (N_I): N_V(control)=589, N_I(control)=179; N_V(0.5% PE-PEG2000)= 1633, N_I(0.5% PE-PEG2000)=238; N_V(0.5% PE-PEG3400)= 1634, N_I(0.5% PE-PEG3400)=242; N_V(0.5% PE-PEG5000)= 1779, N_I(0.5% PE-PEG5000)=215; N_V(5% PE-PEG2000)= 1231, N_I(5% PE-PEG2000)=222. B) Distribution of the diameter of protein-free liposomes measured with CryoEM. Individual measurements were grouped in 50 nm 'bins'. Each data point (circle) represents the relative frequency of each bin. Solid lines represent the fits of the data to a log-normal distribution (Eq. 7). C) Median (<D>) and variance (σ) of the liposome diameter distributions measured with DLS and EM.

Supplementary Figure 4. Determination of the lower bound of the scrambling rate constant for PE in the presence of Ca^{2+}.

A-B) Fluorescence decay of C_6-NBD-PE (A) or *N*-NBD-PE (B) in the presence of 0.5 mM Ca^{2+} (black) are fit to Eq. 5 at fixed values of $\alpha=\beta$; α =0.05 (red), α =0.2 (blue), α =10 (green). C) χ^2 values for the fits from (A) and (B) with α = 0.05, 0.1, 0.2, 0.5, 1, 10 or 1000 for C_6-NBD-PE (white circles) or *N*-NBD-PE (black circles).

Supplementary Figure 5. Phospholipid scrambling by nhTMEM16

A-B) Representative traces of the time course of the fluorescence reduction in nhTMEM16-containing liposomes reconstituted with 0.5 mole% *N*-NBD-PE (A) or 0.5 mole% PE-PEG2000-NBD with 0.5mM Ca^{2+} (red) or 0mM Ca^{2+} (black). Green traces represent protein-free liposomes. Dashed cyan lines represent fits to Eq. 5 or 4. *n*=7-9 * denotes the addition of sodium dithionite.

Supplementary Figure 6. Concentration dependence of the NBD reduction rate of PE-PEG2000-NBD lipids.

A-B) Time course of fluorescence decay of protein-free (A) or afTMEM16-containing liposomes in the presence of 0.5 mM Ca^{2+} reconstituted with 0.5 mole % of PE-PEG2000-NBD upon addition of 20 (green) or 2.5 mM (blue) sodium dithionite. C) NBD reduction rate constant, τ, of PE-PEG2000-NBD by 20 mM (green) or 2.5 mM (blue) sodium dithionite determined by fitting decay traces to Eq. 2 (protein-free) or Eq. 4 (proteoliposomes). In all cases *n*=3. Data is shown as mean ± S.E.M.

Supplementary Figure 7. Proposed ‘’credit card’’ and ‘’out of the groove’’ lipid scrambling mechanisms.

Comparison of the proposed scrambling mechanisms, “credit card” (left) and “out of the groove” (right). For clarity of visualization the two mechanisms are shown separately, however we suggest that they act simultaneously and synergistically. The lipids in the left subunit are shown to be scrambled through the groove (light cyan) according to the credit card mechanism. The groove in the right subunit is shown to locally deform the membrane by thinning it (blue arrows) to allow translocation of all phospholipids outside the cavity. Lipids with normal headgroups are shown in green, those with headgroups larger than the cavity in wheat color.

TABLES

NBD-Lipid	Condition	f_0	α (s^{-1})	β (s^{-1})	γ (s^{-1})	$L_i^{PF}(0)$	*n*
C6-NBD-PE	Protein Free	*n.a.*	*n.a.*	*n.a.*	0.07±0.01	0.53±0.06	23
	afTMEM16 + Ca^{2+}	0.21±0.09	>0.2*		0.11±0.03	0.5	16
	afTMEM16 0 Ca^{2+}	0.32±0.12	$(3.5\pm1.0)\cdot10^{-3}$	$(1.3\pm0.4)\cdot10^{-3}$	0.05±0.01	0.5	14
***N*-NBD-PE**	Protein Free	*n.a.*	*n.a.*	*n.a.*	0.035±0.004	0.46±0.05	11
	afTMEM16 + Ca^{2+}	0.21±0.10	>0.2*		0.06±0.01	0.46	13
	afTMEM16 0 Ca^{2+}	0.2	$(1.5\pm0.8)\cdot10^{-3}$	$(0.7\pm0.3)\cdot10^{-3}$	0.027±0.003	0.46	13
PE-PEG2000-NBD	Protein Free	*n.a.*	*n.a.*	*n.a.*	1.0±0.3	0.50±0.04	22
	afTMEM16 + Ca^{2+}	0.19±0.05	0.11±0.07	0.09±0.09	1	0.5	18
	afTMEM16 0 Ca^{2+}	0.37±0.13	$(1.4\pm0.4)\cdot10^{-3}$	$(1.1\pm0.6)\cdot10^{-3}$	1	0.5	21
PE-PEG3400-NBD	Protein Free	*n.a.*	*n.a.*	*n.a.*	1.0±0.3	0.39±0.04	8
	afTMEM16 + Ca^{2+}	0.23±0.02	>1*		1	0.39	9
	afTMEM16 0 Ca^{2+}	0.52±0.03	$(4\pm4)\cdot10^{-3}$*		1	0.24±0.07	9
PE-PEG5000-NBD	Protein Free	*n.a.*	*n.a.*	*n.a.*	1.0±0.2	0.38±0.04	9
	afTMEM16 + Ca^{2+}	0.32±0.04	>1*		1	0.38	10
	afTMEM16 0 Ca^{2+}	0.24±0.14	$(2.9\pm0.8)\cdot10^{-3}$	$(1.2\pm0.4)\cdot10^{-3}$	1	0.38	10
DA/EA *N*-NBD-PE	Protein Free	*n.a.*	*n.a.*	*n.a.*	0.03±0.003	0.54±0.018	6
	afTMEM16 + Ca^{2+}	0.36±0.09	$(1.7\pm0.7)\cdot10^{-3}$	$(1.2\pm0.6)\cdot10^{-3}$	0.027±0.0025	0.54	6
	afTMEM16 0 Ca^{2+}	0.37±0.01	$(3.6\pm0.5)\cdot10^{-3}$	$(3.3\pm1)\cdot10^{-3}$	0.02±0.0023	0.54	6
DA/EA PE-PEG2000-NBD	Protein Free	*n.a.*	*n.a.*	*n.a.*	0.89±0.09	0.54±0.03	6
	afTMEM16 + Ca^{2+}	0.19±0.07	$(0.8\pm0.1)\cdot10^{-3}$	$(0.5\pm0.08)\cdot10^{-3}$	1.35±0.35	0.54	6
	afTMEM16 0 Ca^{2+}	0.36±0.03	$(1.6\pm0.12)\cdot10^{-3}$	$(0.8\pm0.07)\cdot10^{-3}$	1.19±0.29	0.54	6

Table 1. Average values of the scrambling rate constants of the nested PE headgroup series. The following parameters were derived by fitting the data to Eq. 2, 4 or 5: f_0 is the fraction of empty liposomes, α and β are the forward and backwards scrambling rate constants, γ is the reduction rate constant by dithionite, L_i^{PF} is the fraction of NBD-labeled lipids in the inner leaflet of a protein-free vesicle, n is the number of independent experiments. * denotes cases where the values of α and β could not be determined from the fit. In this case we imposed that $\alpha=\beta$, Eq. 5 was used to fit the time course, and their value was constrained to the lower bound on the rate constant as described in Suppl. Fig. 5. Protein free traces were fit to Eq. 2. In all other cases Eq. 4 was used. All data is reported as the mean ± Standard deviation of the parameters derived from the fits of *n* individual traces. Where no error is indicated it means that the parameter was kept fixed to the corresponding experimentally determined protein-free value.

NBD-Lipid	Condition	f_0	α (s^{-1})	β (s^{-1})	γ (s^{-1})	$L_i^{PF}(0)$	*n*
***N*-NBD-PE**	Protein Free	*n.a.*	*n.a.*	*n.a.*	0.053±0.0096	0.57±0.02	9
	nhTMEM16 + Ca^{2+}	0.35±0.040	>0.2*		0.058±0.007	0.57	9
	nhTMEM16 0 Ca^{2+}	0.47±0.05	$(2.38±0.73)\cdot10^{-3}$	$(1.41±0.68)\cdot10^{-3}$	0.04±0.0065	0.57	8
	R432W + Ca^{2+}	0.46±0.07	$(2.09±0.38)\cdot10^{-3}$	$(1.6±0.62)\cdot10^{-3}$	0.047±0.0067	0.57	9
	R432W 0 Ca^{2+}	0.53±0.16	$(0.53±0.4)\cdot10^{-3}$	$(0.42±0.09)\cdot10^{-3}$	0.048±0.007	0.57	7
PE-PEG2000-NBD	Protein Free	*n.a.*	*n.a.*	*n.a.*	1.02±0.26	0.61±0.06	8
	nhTMEM16 + Ca^{2+}	0.25±0.06	0.016±0.01	0.0032±0.01	1.02	0.61	8
	nhTMEM16 0 Ca^{2+}	0.3±0.06	$(1.31±0.35)\cdot10^{-3}$	$(1.28±0.4)\cdot10^{-3}$	1.02	0.61	7
	R432W + Ca^{2+}	0.22±0.05	$(1.78±0.89)\cdot10^{-3}$	$(2.25±0.52)\cdot10^{-3}$	1.02	0.61	8
	R432W 0 Ca^{2+}	0.17±0.066	$(0.24±0.03)\cdot10^{-3}$	$(0.38±0.13)\cdot10^{-3}$	1.02	0.61	7

Table 2. Average values of the scrambling rate constants of nhTMEM16

The following parameters were derived by fitting the data to Eq. 2, 4 or 5: f_0 is the fraction of empty liposomes, α and β are the forward and backwards scrambling rate constants, γ is the reduction rate constant by dithionite, $L_i^{PF}(0)$ is the fraction of NBD-labeled lipids in the inner leaflet of a protein-free vesicle, n is the number of independent experiments. * denotes cases where the values of α and β could not be determined from the fit. In these case we imposed that α=β, Eq. 5 was used to fit the time course, and their value was constrained to the lower bound on the rate constant as described in Suppl. Fig. 5. Protein free traces were fit to Eq. 2. In all other cases Eq. 4 was used. All data is reported as the mean ± Standard deviation of the parameters derived from the fits of *n* individual traces. Where no error is indicated it means that the parameter was kept fixed to the corresponding experimentally determined protein-free value.

NBD-Lipid	Condition	τ (s)	L (s^{-1})	P	*n*
***N*-NBD-PE**	Protein Free	48.2 ± 1.3	$(7.53 \pm 0.21) \cdot 10^{-5}$	0.56 ± 0.01	3
	Opsin	58 ± 1	$(10.1 \pm 0.1) \cdot 10^{-5}$	0.32 ± 0.01	3
PE-PEG2000-NBD	Protein Free	1.5 ± 0.3	$(9.33 \pm 0.43) \cdot 10^{-5}$	0.46 ± 0.01	3
	Opsin	1.22 ± 0.05	$(27.4 \pm 0.1) \cdot 10^{-5}$	0.31 ± 0.01	3

Table 3. Quantification of scrambling by opsin. Fit parameters of the opsin fluorescence decay time course described with Eq. 6. Data is mean±S.E.M.

Appendix 1

The time course of fluorescence decay post-dithionite addition of a liposome containing at least one active scramblase is described by a 3-state Markov model (2)

$$L_i \underset{\beta}{\overset{\alpha}{\rightleftarrows}} L_o \xrightarrow{\gamma} L^*$$

Where L_i and L_o are the fluorescent NBD-labeled lipids in the inner and outer leaflet of a membrane, L* is their dithionite reduced, non-fluorescent form, α and β are the forward and backwards scrambling rate constants, γ is the pseudo-first order rate constant of dithionite reduction of an NBD fluorophore conjugated to a lipid, and γ =[D]γ', where [D] is the dithionite concentration and γ' is the second order rate constant for dithionite reduction. Therefore, the time evolution of the fluorescence signal of a vesicle containing at least one active scramblase, $F_{Scr}(t)$, is given by:

$$F_{Scr}(t) = Li(t) + Lo(t) \qquad \text{(Eq. A1)}$$

The time variation of each component is given by:

$$\frac{dL_i(t)}{dt} = -\alpha Li(t) + \beta Lo(t) \qquad \text{(Eq. A2)}$$

$$\frac{dL_o(t)}{dt} = \alpha Li(t) - (\beta + \gamma) Lo(t) \qquad \text{(Eq. A3)}$$

Writing Eq. A2 and A3 in matrix form we get that

$$\frac{d}{dt}\begin{pmatrix} Li(t) \\ Lo(t) \end{pmatrix} = \begin{pmatrix} -\alpha & \beta \\ \alpha & -(\beta+\gamma) \end{pmatrix}\begin{pmatrix} Li(t) \\ Lo(t) \end{pmatrix} = M\bar{L}(t) \qquad \text{(Eq. A4)}$$

Where M is a 2x2 matrix and $\bar{L}(t)$ is the vector with components $L_{i,o}(t)$.

Since Eq. A4 is a system of homogeneous linear differential equations of the first order the solution will be

$$\bar{L}(t) = \hat{v}_1 A e^{\lambda_1 t} + \hat{v}_1 B e^{\lambda_2 t} \qquad \text{(Eq. A5)}$$

Where $\hat{v}_{1,2}$ and $\lambda_{1,2}$ are respectively the eigenvectors and eigenvalues of M. To identify the eigenvalues of M we impose that

$$|\mathrm{M} - \lambda \mathrm{I}| = \begin{vmatrix} -\alpha - \lambda & \beta \\ \alpha & -(\beta+\gamma) - \lambda \end{vmatrix} = \begin{vmatrix} -(\alpha+\lambda) & \beta \\ \alpha & -(\beta+\gamma+\lambda) \end{vmatrix} = 0$$

Where I is the unitary matrix, so that

$$\lambda_1 = -\frac{(\alpha+\beta+\gamma) - \sqrt{(\alpha+\beta+\gamma)^2 - 4\alpha\gamma}}{2} \quad \text{and} \quad \lambda_2 = -\frac{(\alpha+\beta+\gamma) + \sqrt{(\alpha+\beta+\gamma)^2 - 4\alpha\gamma}}{2} \qquad \text{(Eq. A6)}$$

To identify the eigenvectors, we impose that

$$M\hat{v}_{1,2} = \lambda_{1,2}\hat{v}_{1,2}$$

To find $\widehat{v_1}$we impose that

$$\begin{pmatrix} -\alpha & \beta \\ \alpha & -(\beta+\gamma) \end{pmatrix} \begin{pmatrix} X \\ Y \end{pmatrix} = \lambda_1 \begin{pmatrix} X \\ Y \end{pmatrix}$$

So that

$$\hat{v}_1 = \begin{pmatrix} \beta \\ \lambda_1 + \alpha \end{pmatrix}$$

Similarly, we find that

$$\hat{v}_2 = \begin{pmatrix} \lambda_2 + \beta + \gamma \\ \alpha \end{pmatrix}$$

$$\hat{v}_1 = \begin{pmatrix} \beta \\ \lambda_1 + \alpha \end{pmatrix} \qquad \text{and} \qquad \hat{v}_2 = \begin{pmatrix} \lambda_2 + \beta + \gamma \\ \alpha \end{pmatrix} \quad \text{(Eq. A7)}$$

Replacing the expressions for $\hat{v}_{1,2}$into Eq. A4 we get

$$\begin{pmatrix} Li(t) \\ Lo(t) \end{pmatrix} = \begin{pmatrix} \beta \\ \lambda_1 + \alpha \end{pmatrix} Ae^{\lambda_1 t} + \begin{pmatrix} \lambda_2 + \beta + \gamma \\ \alpha \end{pmatrix} Be^{\lambda_2 t} \quad \text{(Eq. A8)}$$

Where A and B are two constants. So that the time evolution of the individual components can be written as

$$L_i(t) = \beta A e^{\lambda_1 t} + (\lambda_2 + \beta + \gamma) B e^{\lambda_2 t} \qquad \text{(Eq. A9)}$$

$$L_o(t) = (\lambda_1 + \alpha) A e^{\lambda_1 t} + \alpha B e^{\lambda_2 t} \qquad \text{(Eq. A10)}$$

And the time evolution of the fluorescence decay is

$$F_{Scr}(t) = (\lambda_1 + \alpha + \beta) A e^{\lambda_1 t} + (\lambda_2 + \alpha + \beta + \gamma) B e^{\lambda_2 t} \quad \text{(Eq. A11)}$$

Since Eq. A3 is an homogeneous set of first order differential equations we can use the initial conditions of the system to determine A and B. Let the initial values of the fraction of the lipids in the inner and outer leaflet be $L_i(0)$ and $L_o(0)$, with

$$L_i(0)+L_o(0)=1$$

So that Eq. A9 and A10 at t=0 become

$$L_i(0) = \beta A + (\lambda_2 + \beta + \gamma) B$$

$$L_o(0) = (\lambda_1 + \alpha) A + \alpha B$$

We can solve the first relationship for A we get that

$$A = \frac{L_i(0) - (\lambda_2 + \beta + \gamma) B}{\beta}$$

And substituting into the second to find

$$L_o(0) = \frac{(\lambda_1 + \alpha)}{\beta} L_i(0) - \left[\frac{(\lambda_1 + \alpha)(\lambda_2 + \beta + \gamma) - \alpha\beta}{\beta} \right] B$$

Let us call

$$D = (\lambda_1 + \alpha)(\lambda_2 + \beta + \gamma) - \alpha\beta$$

Solving for B we get

$$B = \frac{(\lambda_1 + \alpha)Li(0) - \beta Lo(0)}{D}$$

And

$$A = \frac{(\lambda_2 + \beta + \gamma) - (\lambda_2 + \alpha + \beta + \gamma)Li(0)}{D}$$

Replacing these expressions into Eq. A9, A10 and A11 we obtain that

$$L_i(t) = \beta\frac{(\lambda_2+\beta+\gamma)-(\lambda_2+\alpha+\beta+\gamma)Li(0)}{D}e^{\lambda_1 t} + (\lambda_2 + \beta + \gamma)\frac{(\lambda_1+\alpha+\beta)Li(0)-\beta}{D}e^{\lambda_2 t} \qquad \text{(Eq. A12)}$$

$$L_o(t) = (\lambda_1 + \alpha)\frac{(\lambda_2+\beta+\gamma)-(\lambda_2+\alpha+\beta+\gamma)Li(0)}{D}e^{\lambda_1 t} + \alpha\frac{(\lambda_1+\alpha+\beta)Li(0)-\beta}{D}e^{\lambda_2 t} \quad \text{(Eq. A13)}$$

$$F_{Scr}(t) = \frac{1}{D}\{(\lambda_1 + \alpha + \beta)[(\lambda_2 + \beta + \gamma) - (\lambda_2 + \alpha + \beta + \gamma)Li(0)]e^{\lambda_1 t} + (\lambda_2 + \alpha + \beta + \gamma)[(\lambda_1 + \alpha + \beta)Li(0) - \beta]e^{\lambda_2 t}\} \qquad \text{(Eq. A14)}$$

Importantly, at the time of dithionite addition (t=0 in the time evolution) we can assume that the system is in the equilibrium state created by the scramblases. This implies that $L_i(0)$ and $L_o(0)$ are related through α and β by the equilibrium relationship, so that

$$\frac{L_i(0)}{L_o(0)} = \frac{\beta}{\alpha}$$

This, with the consideration that $L_i(0) + L_o(0) = 1$ gives that

$$L_i(0) = \frac{\beta}{\alpha+\beta} \quad L_o(0) = \frac{\alpha}{\alpha+\beta}$$

Thus Eq. A14 becomes

$$F_{Scr}(t) = \frac{\{\alpha(\lambda_2+\gamma)(\lambda_1+\alpha+\beta)e^{\lambda_1 t}+\lambda_1\beta(\lambda_2+\alpha+\beta+\gamma)e^{\lambda_2 t}\}}{D(\alpha+\beta)} \qquad \text{(Eq. A15)}$$

In our system not all vesicles contain one active scramblase, there is a fraction, f_0, that is refractory to protein incorporation. These protein-free vesicles will also contribute to the time-dependent fluorescence signal as their outer-leaflet NBD-lipids are reduced by dithionite with a single exponential time course described by

$$F_{PF}(t) = (L_i^{PF} + (1 - L_i^{PF})e^{-\gamma t}) \qquad \text{(Eq. A16)}$$

Where L_i^{PF} is the fraction of NBD-lipids in the inner leaflet of the membrane of protein-free liposomes.

Thus, by fitting the time course of the fluorescence decay of protein-free liposomes we can experimentally determine L_i^{PF} and γ. Therefore, the total fluorescence signal is given by weighted the sum of the fluorescence of the two vesicle populations described in Eq. A15 and A16

$$F_{tot}(t) = f_0 \mathrm{F}_{PF}(\mathrm{t}) + (1 - f_0)F_{Scr}(t) \qquad \text{(Eq. A17)}$$

Substituting Eq. A15 and A16 into Eq. A17 we find that the time evolution of the total fluorescence of the system is described by

$$F_{tot}(t) = f_0(L_i^{PF} + (1 - L_i^{PF})e^{-\gamma t}) + \frac{(1-f_0)}{D(\alpha+\beta)}\{\alpha(\lambda_2 + \gamma)(\lambda_1 + \alpha + \beta)e^{\lambda_1 t} + \lambda_1\beta(\lambda_2 + \alpha + \beta + \gamma)e^{\lambda_2 t}\} \qquad \text{(Eq. A18)}$$

If we can make the simplifying assumption that the forward and backwards rates of scrambling are equal and that in protein-free liposomes the lipids distribute equally in the two leaflets

$$\alpha=\beta \quad \text{and} \quad L_i^{PF}=L_o^{PF}=0.5$$

Eq. A18 then simplifies to

$$F_{tot}(t) = \frac{f_0}{2}(1 + e^{-\gamma t}) + \frac{(1-f_0)}{2D}\left[(\lambda_2 + \gamma)(\lambda_1 + 2\alpha)e^{\lambda_1 t} + \lambda_1(\lambda_2 + 2\alpha + \gamma)e^{\lambda_2 t}\right] \quad \text{(Eq. A19)}$$

With

$$\lambda_1 = -\frac{(2\alpha+\gamma)-\sqrt{4\alpha^2+\gamma^2}}{2} \qquad \lambda_2 = -\frac{(2\alpha+\gamma)+\sqrt{4\alpha^2+\gamma^2}}{2} \qquad D = (\lambda_1 + \alpha)(\lambda_2 + \alpha + \gamma) - \alpha^2$$

It is important to note that these assumptions will hold if the scramblases reconstitute with equal probability in both orientations in the vesicles and if there is no preferential direction of transport. However, in the presence of asymmetric starting conditions, such as those seen with some PEG-conjugated lipids, or in the presence of “leaks” (due to imperfect sealing of the liposomes allowing spontaneous lipid flipping or slow entry of dithionite) these assumptions might not hold true.

REFERENCES

1. Malvezzi M, *et al.* (2013) Ca2+-dependent phospholipid scrambling by a reconstituted TMEM16 ion channel. *Nat Commun* 4:2367.
2. Marx U, *et al.* (2000) Rapid flip-flop of phospholipids in endoplasmic reticulum membranes studied by a stopped-flow approach. *Biophys J* 78(5):2628-2640.

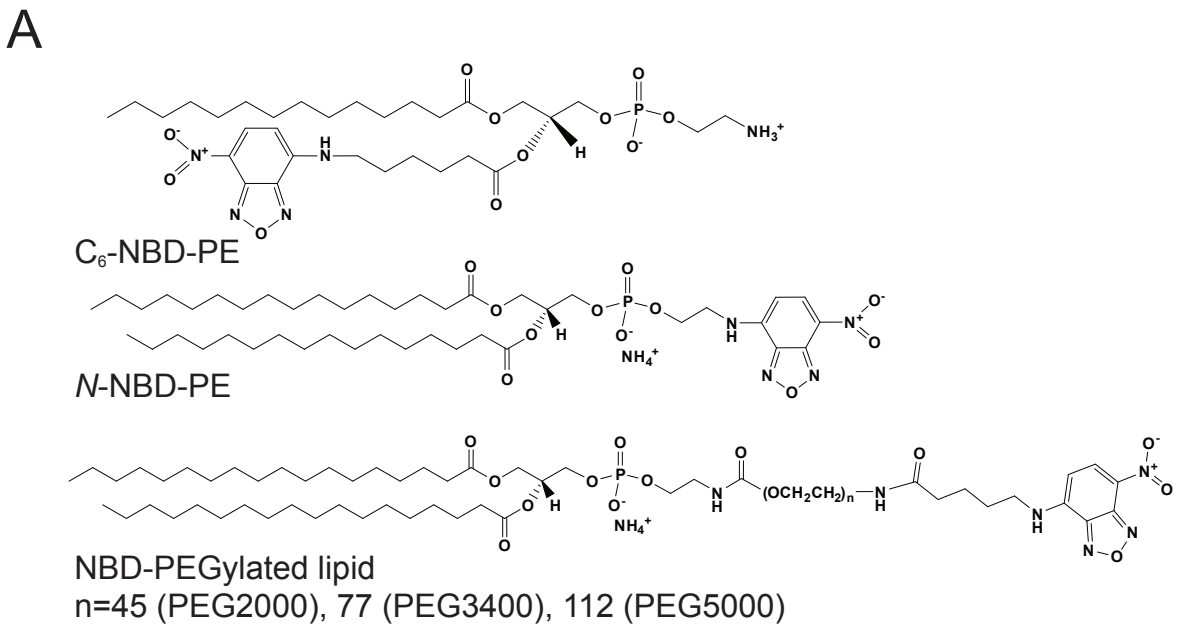
A
C6-NBD-PE
N-NBD-PE
NBD-PEGylated lipid
n=45 (PEG2000), 77 (PEG3400), 112 (PEG5000)

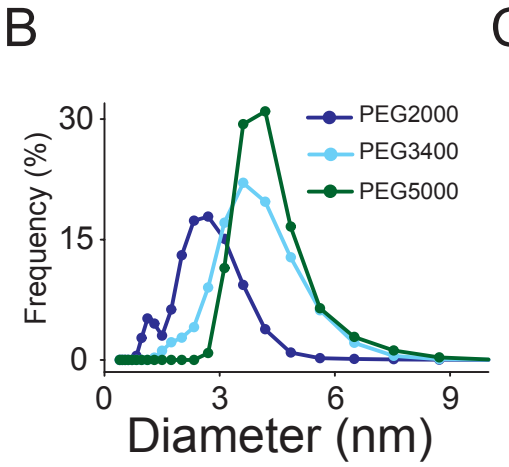
B
PEG2000
PEG3400
PEG5000
Frequency (%)
Diameter (nm)

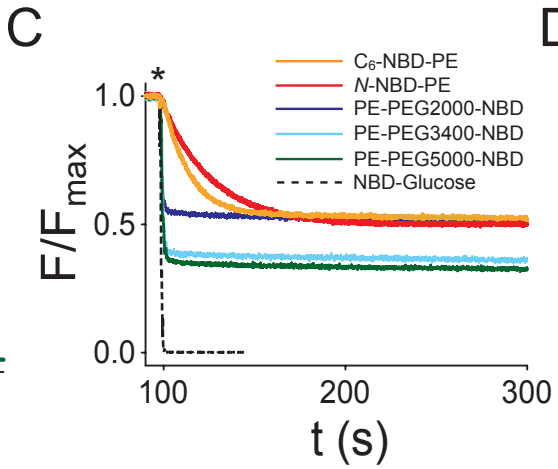
C
C6-NBD-PE
N-NBD-PE
PE-PEG2000-NBD
PE-PEG3400-NBD
PE-PEG5000-NBD
NBD-Glucose
F/Fmax
t (s)

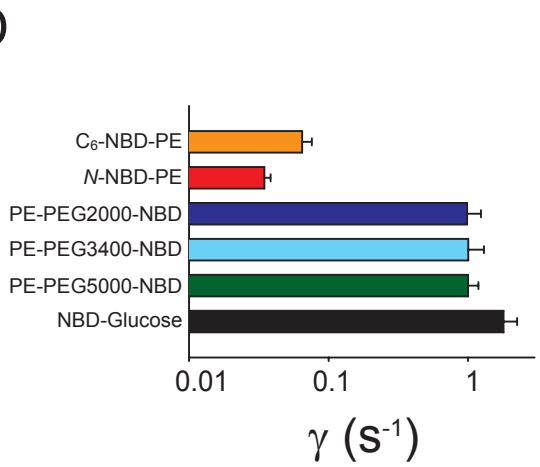
D
C6-NBD-PE
N-NBD-PE
PE-PEG2000-NBD
PE-PEG3400-NBD
PE-PEG5000-NBD
NBD-Glucose
γ (s-1)

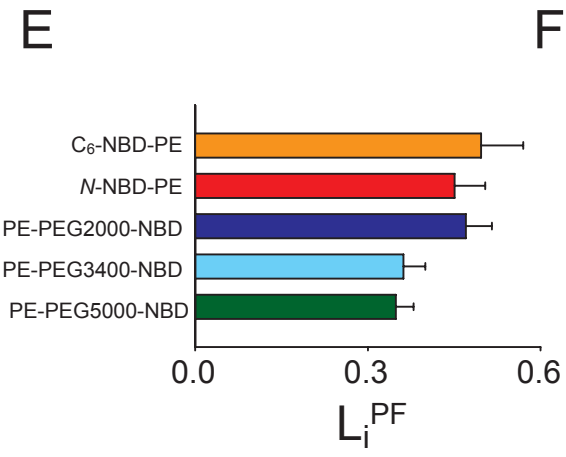
E
C6-NBD-PE
N-NBD-PE
PE-PEG2000-NBD
PE-PEG3400-NBD
PE-PEG5000-NBD
Li PF

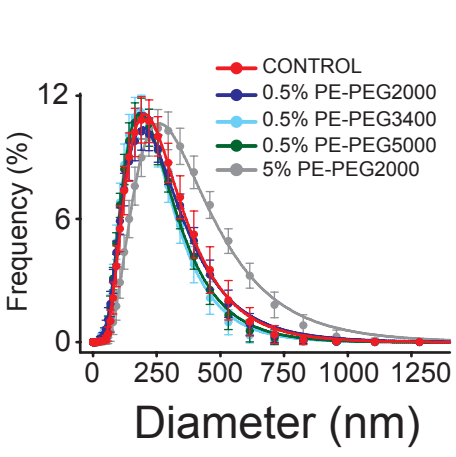
F
CONTROL
0.5% PE-PEG2000
0.5% PE-PEG3400
0.5% PE-PEG5000
5% PE-PEG2000
Frequency (%)
Diameter (nm)

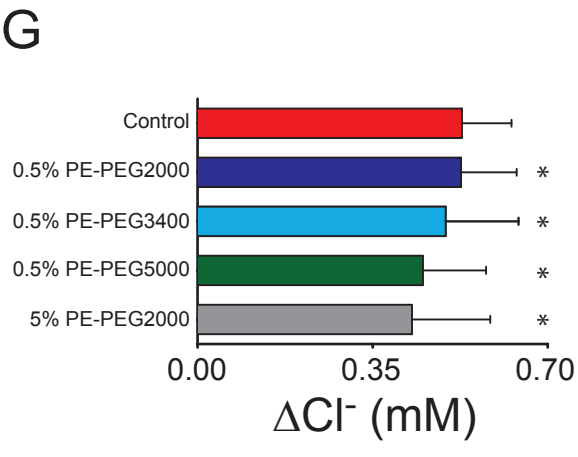
G
Control
0.5% PE-PEG2000
0.5% PE-PEG3400
0.5% PE-PEG5000
5% PE-PEG2000
ΔCl- (mM)

A

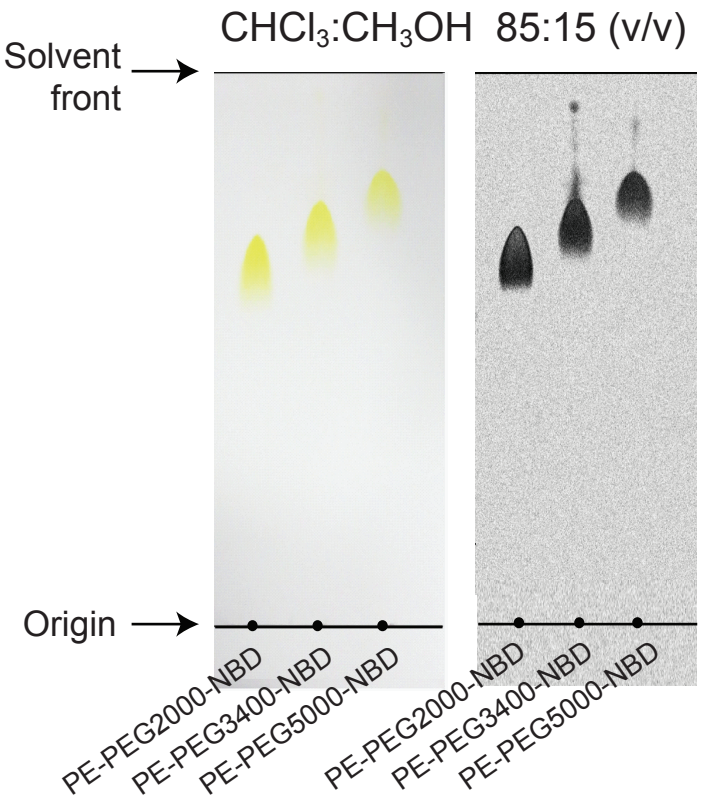

B

DPSE-PEG-NBD Lipid (Da)	Expected Mass (Da)	Mass Spec Data (Da) Peak Max ± FWHM
PE-PEG2000-NBD	3050	3052 ± 150
PE-PEG3400-NBD	4467	4496 ± 500
PE-PEG5000-NBD	6067	6052 ± 640

A

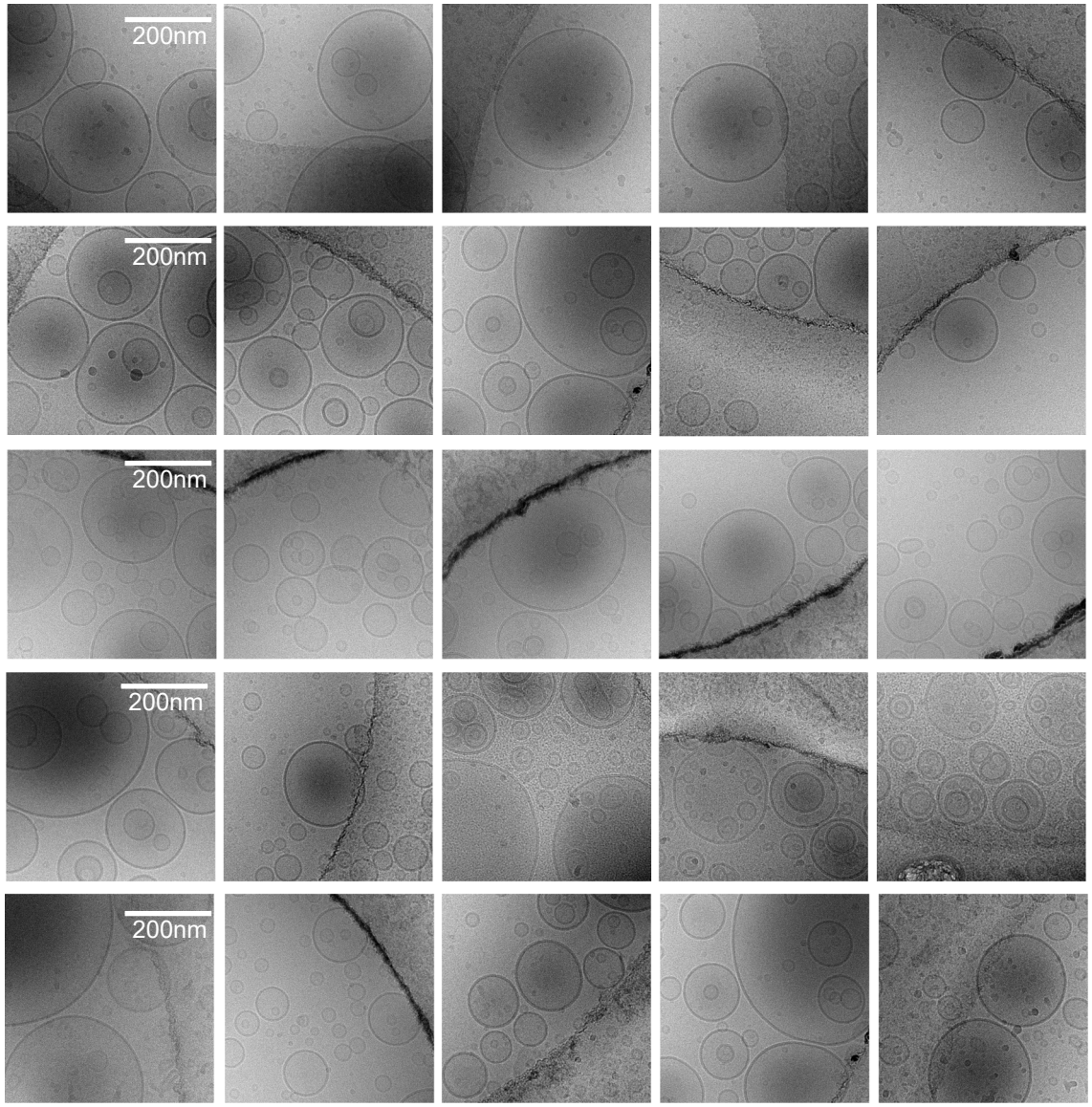

B

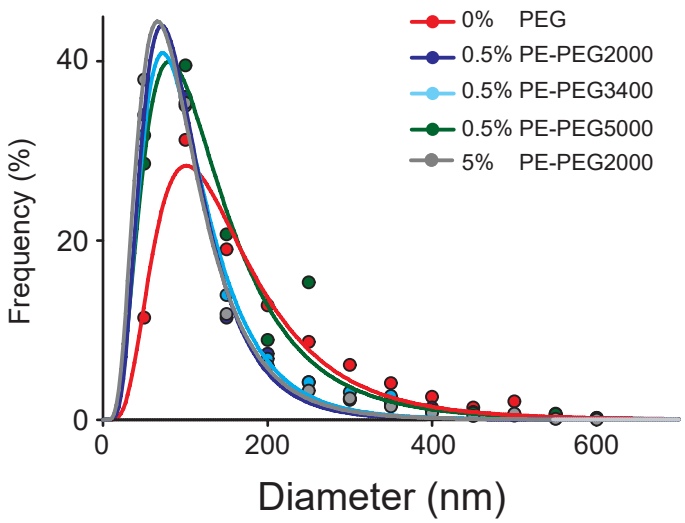

C

Condition	DLS		EM	
	<D> (nm)	σ (nm)	<D> (nm)	σ (nm)
Control	202	134	101	72
+0.5% PE-PEG2000	195	140	71	43
+0.5% PE-PEG3400	182	116	73	48
+0.5% PE-PEG5000	185	122	81	64
+5% PE-PEG2000	261	184	66	61

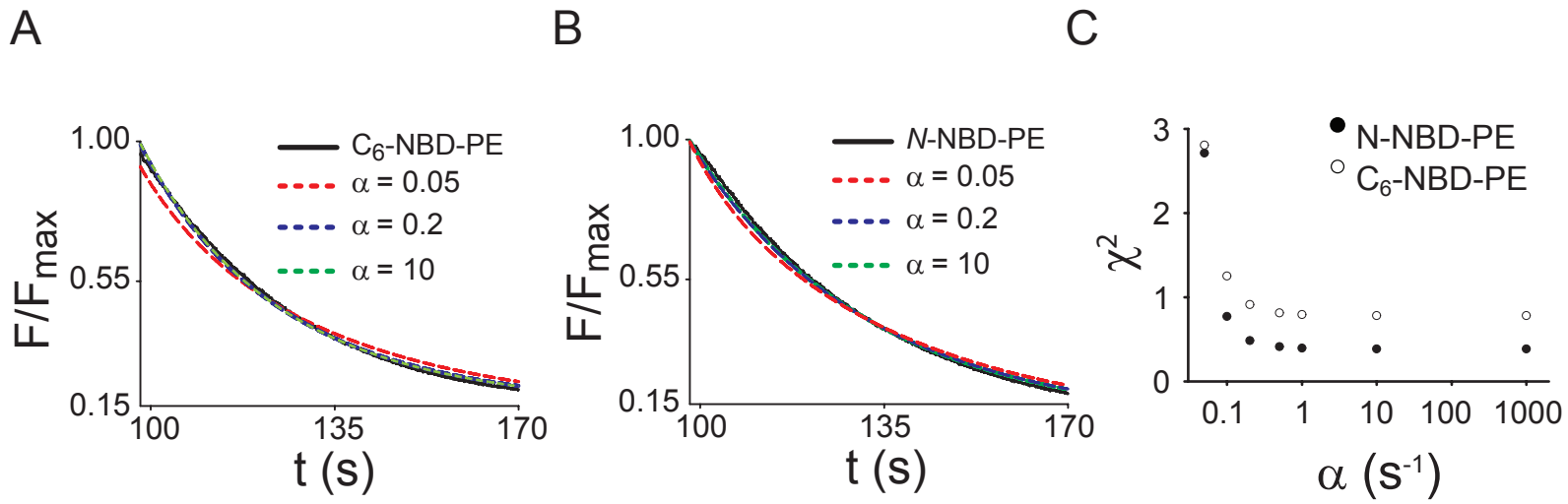
A
B
C
1.00
0.55
0.15
F/F_max
100
135
170
t (s)
C6-NBD-PE
α = 0.05
α = 0.2
α = 10
N-NBD-PE
3
2
1
0
χ2
0.1
1
10
100
1000
α (s-1)

A

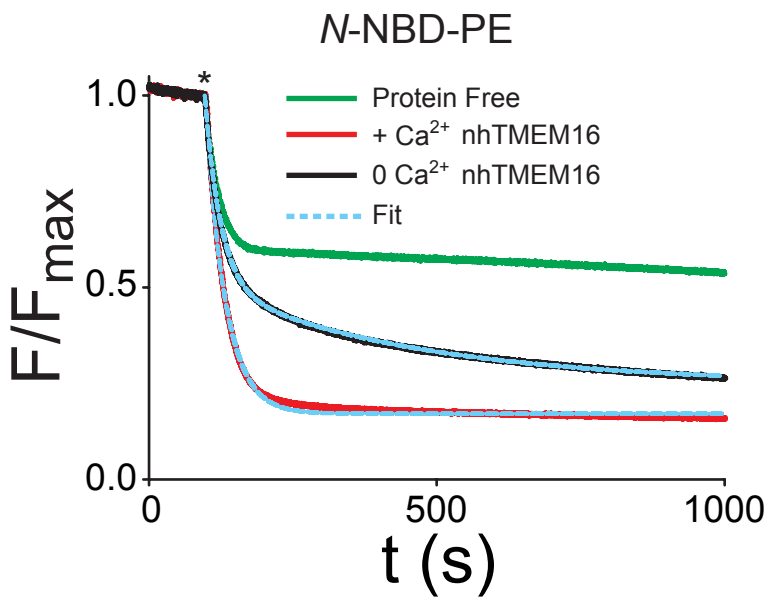
N-NBD-PE
1.0
0.5
0.0
F/Fmax
0
500
1000
t (s)
*
Protein Free
+ Ca2+ nhTMEM16
0 Ca2+ nhTMEM16
Fit

B

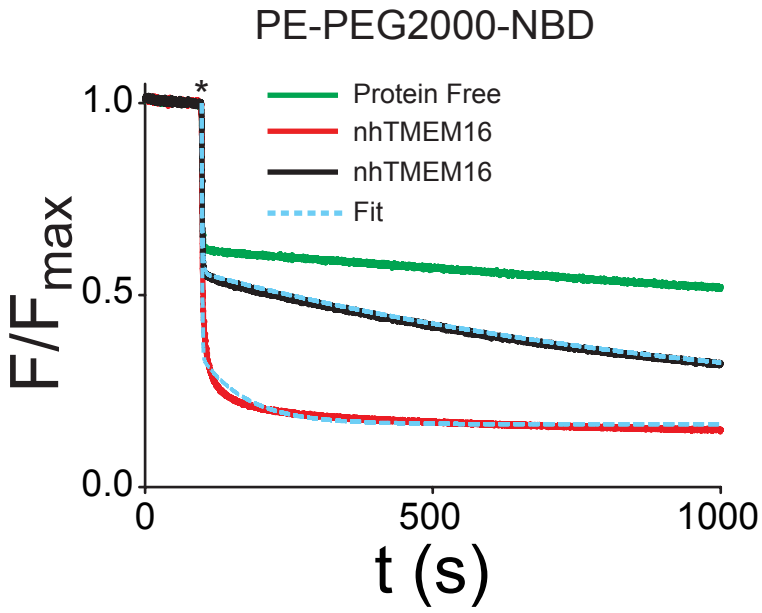
PE-PEG2000-NBD
1.0
0.5
0.0
F/Fmax
0
500
1000
t (s)
*
Protein Free
nhTMEM16
nhTMEM16
Fit

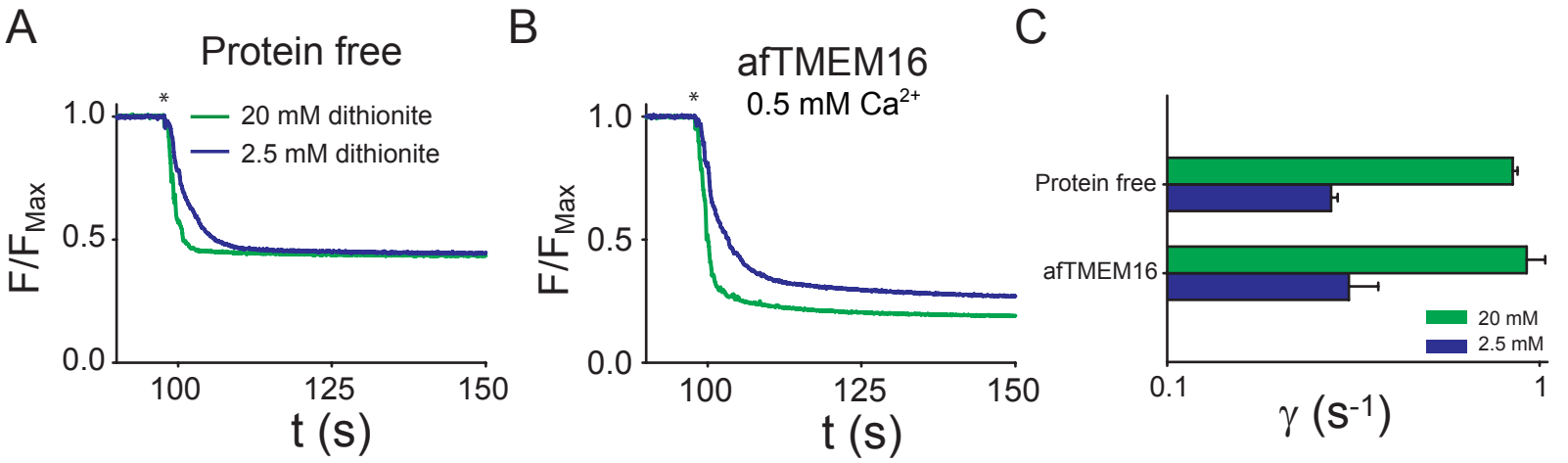
A
Protein free
20 mM dithionite
2.5 mM dithionite
F/F_Max
t (s)
B
afTMEM16
0.5 mM Ca2+
C
Protein free
afTMEM16
20 mM
2.5 mM
γ (s-1)

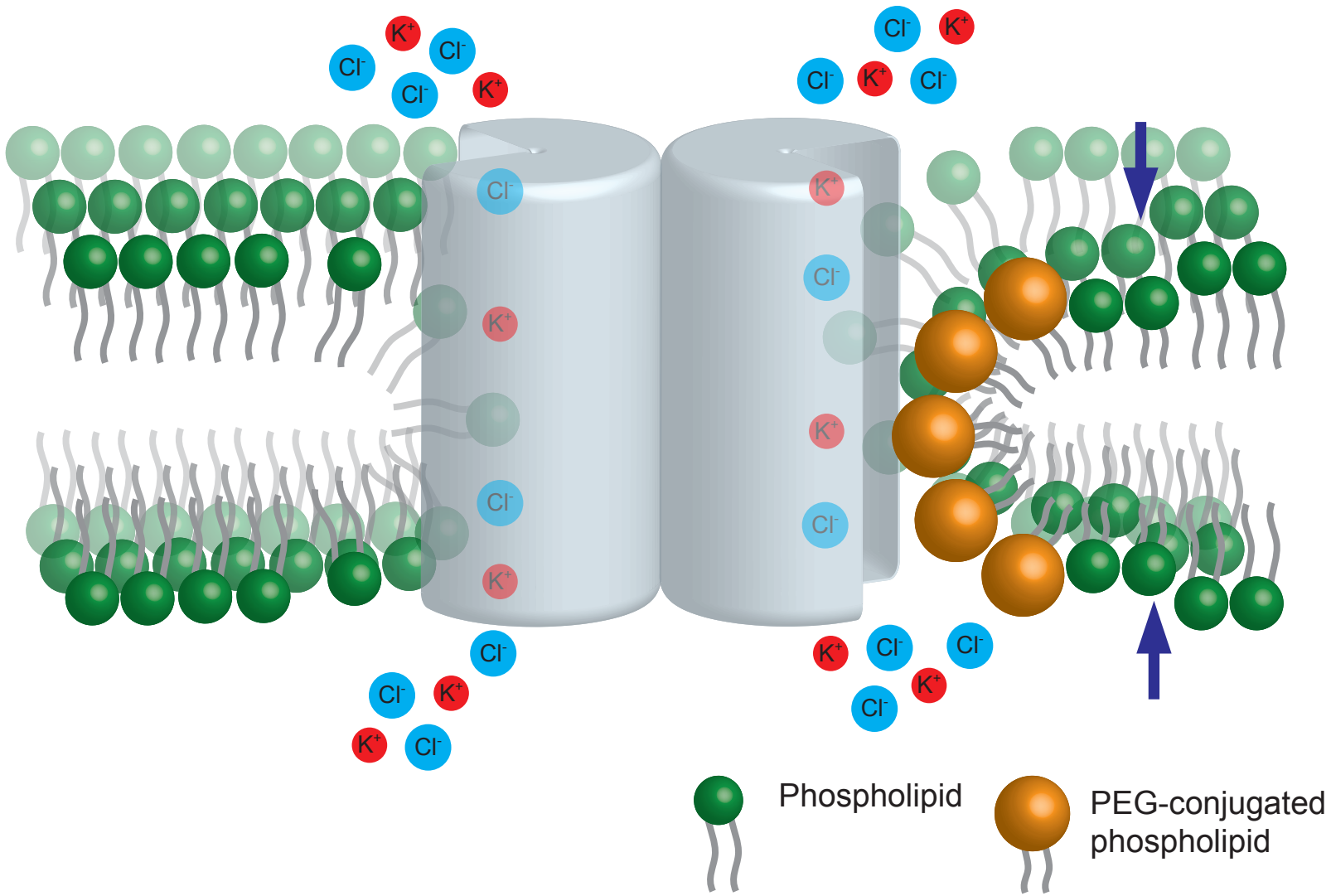
K+
Cl-
Phospholipid
PEG-conjugated
phospholipid